Journal of African Earth Sciences 57 (2010) 14–30

Contents lists available at ScienceDirect

Journal of African Earth Sciences

journal homepage: www.elsevier.com/locate/jafrearsci

Geochemistry and mineralogy of Cu and Co in mine tailings at the Copperbelt, Zambia

O. Sracek [a,b,*], M. Mihaljevič [c], B. Kříbek [d], V. Majer [d], F. Veselovský [d]

[a] OPV s.r.o. (Protection of groundwater Ltd.), Břevnovská 31, 169 00 Praha 6, Czech Republic
[b] Department of Geology, Faculty of Science, Palacký University, 17. listopadu 12, 771 46 Olomouc, Czech Republic
[c] Institute of Geochemistry, Mineralogy and Mineral Resources, Faculty of Science, Charles University, Albertov 6, 128 43 Praha 2, Czech Republic
[d] Czech Geological Survey, Klárov 3, 118 21 Praha 1, Czech Republic

ARTICLE INFO

Article history:
Received 23 February 2009
Received in revised form 16 July 2009
Accepted 23 July 2009
Available online 30 July 2009

Keywords:
Zambia
Copperbelt
Mine tailings
Neutralization
Metals
Hardpan

ABSTRACT

Two sulfidic mine tailings within the Zambian Copperbelt in the north of Zambia have been studied: Chambishi, representing an old site (age about 40 y) and Mindolo, which represents a relatively recent site (age less than 10 y). The neutralization capacity based on solid phase carbonates at both sites remains high, thus neutral to alkaline conditions (paste pH up to 8.5 at Chambishi and up to 6.9 at Mindolo) predominate. Pore water at Chambishi has 568 mg/l of Ca and 1820 mg/l of sulfate, but concentrations of Fe and Mn are below 0.1 mg/l and concentrations of Cu and Co are below 0.05 mg/l. The principal secondary minerals at both sites are gypsum, poorly crystalline Fe(III) phases and hematite. Secondary Fe(III) phases are found as mineral coatings or completely replaced primary sulfides like pyrite and chalcopyrite and include large quantities of copper and cobalt in surface rims (up to 7.0 wt.% of Cu and up to 2.0 wt.% of Co). The presence of Fe(III) phases is marked by red color of mine tailings material, which is observed even below the expected penetration of the sulfide oxidation front. This may be explained by reductive dissolution of Fe(III) phases caused by flooding of tailings and temporarily reducing conditions during rainy period, when dissolved iron is transported by infiltrating water to the deeper zone of mine tailings, where it re-precipitates later. At the Chambishi site, precipitation of secondary minerals resulted in an early stage of hardpan formation at 0.6–0.9 m depth, composed mostly of gypsum and hematite. This zone also corresponds to maximum solid phase contents of Cu and Co. No such hardpans were found at the relatively young Mindolo site, where red tailings material, which includes poorly crystalline Fe(III) phases and hematite, is present only in discrete banded zones at several depth levels. Based on geochemical modeling results at the Mindolo site, precipitation of secondary Cu phases such as brochantite and malachite is likely in the zone of evaporation enrichment close to the mine tailings surface. At both the Chambishi and Mindolo sites, there does not seem to be a threat of acid mine drainage formation even over the long-term. Furthermore, the Cu and Co incorporated in hematite seem to be immobilized within the mine tailings.

1. Introduction

Acid mine drainage (AMD) from sulfidic mining wastes is a serious environmental problem. It has been studied in several countries around the world including Canada (McGregor et al., 1998; Johnson et al., 2000; Lefebvre et al., 2001; Sracek et al., 2004; Salzsauer et al., 2005), Sweden (Strömberg and Banwart, 1999; Salmon and Malmström, 2004), Peru (Smuda et al., 2007), Russia (Gieré et al., 2003), and Australia (Ritchie, 1994). The mine drainage waters typically have low pH and high concentrations of sulfate, iron and other metals (Blowes et al., 2003). However, when the neutralization capacity of waste rock highly exceeds its acid generation potential, the resulting pH is neutral and there is a high concentration of sulfate, but low concentration of iron in the drainage waters. Under neutral and oxidizing conditions, iron precipitates as oxyhydroxides on the surface of sulfides such as pyrite, which limits further pyrite oxidation (Nicholson et al., 1990; Hossner and Doolittle, 2003) and also adsorbs released metals (Blowes et al., 1998; Romero et al., 2006). Also, neutral pH conditions have an impact on bacterial populations, when neutrophilic bacteria are most common instead of pyrite oxidizing bacteria, thus further slowing down the pyrite oxidation rate (Blowes et al., 1998).

When the rate of sulfide oxidation is high, cemented layers (hardpans) may form in the unsaturated zone (Blowes et al., 1991; McGregor and Blowes, 2002). The composition of the layers depends on pore water chemistry and the redox status. In acidic

* Corresponding author. Address: OPV s.r.o. (Protection of groundwater Ltd.), Břevnovská 31, 169 00 Praha 6, Czech Republic. Tel.: +420 220515042.
E-mail address: srondra@yahoo.com (O. Sracek).

1464-343X/$ - see front matter © 2009 Elsevier Ltd. All rights reserved.
doi:10.1016/j.jafrearsci.2009.07.008

mine tailings, hardpans are composed of minerals like melanterite, $FeSO_4 \cdot 7H_2O$, and jarosite, $KFe_3(SO_4)_2(OH)_6$. In neutralized mine tailings, typical hardpan minerals are goethite, FeOOH, and gypsum, $CaSO_4 \cdot 2H_2O$. The presence of a hardpan in a vertical profile generally results in increasing bulk density and decreasing porosity. These hardpan layers are very important in the mitigation of mine drainage because (a) they limit the penetration of oxygen to un-oxidized sulfides in deeper zones, and (b) they may incorporate large quantities of metals adsorbed and/or co-precipitated with secondary hardpan minerals (Gilbert et al., 2003). However, the long term stability of hardpans has been questioned (Lottermoser and Ashley, 2006).

This study took place in the so-called Copperbelt in the north of Zambia (Fig. 1). This region is characterized by the rocks of the Katanga system, which were formed during the Neoproterozoic Age (600–544 Ma) as a part of the Kibaran Mobile Belt (KMB) trending towards northeast. The geology comprises argillaceous and carbonate shale, limestone and dolomite of the Upper Roan, Mwashia, Kakontwe and Kundelungu formations (Binda, 1994; Porada and Berhorst, 2000; Rainaud et al., 2005). New geochronological data indicate that metasedimentary rocks of the Katanga Supergroup were deformed and metamorphosed up to eclogite and talc-kyanite white schist facies during the Pan-African Lufilian Orogeny at between ca. 600 and 480 Ma. Regional uplift and cooling that affected the whole Katangan Basin is dated at between 495 and 480 Ma (Rainaud et al., 2002). The uplift was accompanied by the formation of ENE-directed thrusting and later by strike-slip faulting.

Copperbelt-type ores are stratiform to stratabound, characterized by finely disseminated copper–cobalt–iron sulfides (predominantly chalcopyrite, $CuFeS_2$, cobaltiferous pyrite, $Fe(Co)S_2$, and bornite, Cu_5FeS_4, ±carrolite, $Cu(Co,Ni)_2S_4$) in host rocks that may include quartzite (arkose), shale and dolomite deposited in a continental rift environment (Mendelsohn, 1961). The ore grade average is 3 wt.% for Cu and 0.18 wt.% for Co. The genetic models include syndiagenetic, hydrothermal-epigenetic and metamorphic variants. The recent comprehensive study of the copper–cobalt deposits of the Zambian Copperbelt (McGowan et al., 2006) based on ore mineralogy, hydrothermal alterations, and stable isotopic data lends support to models consistent with the thermo-chemical reduction of a sulfate- (and metal) enriched hydrothermal fluids at the sites of mineralization.

The mining is focused on the recovery of copper and cobalt by flotation processes and smelting. Large volumes of mine tailings material are deposited in ponds and the resulting mine drainage typically has a neutral pH due to a high neutralization capacity of the parent rocks and liming prior to tailings deposition (von der Heyden and New, 2005).

This study describes conditions at two mine tailings sites (Fig. 1): Chambishi, which represents an older mine tailings (age about 40 y) and Mindolo, which represents a relatively young mine tailings (age less than 10 y).

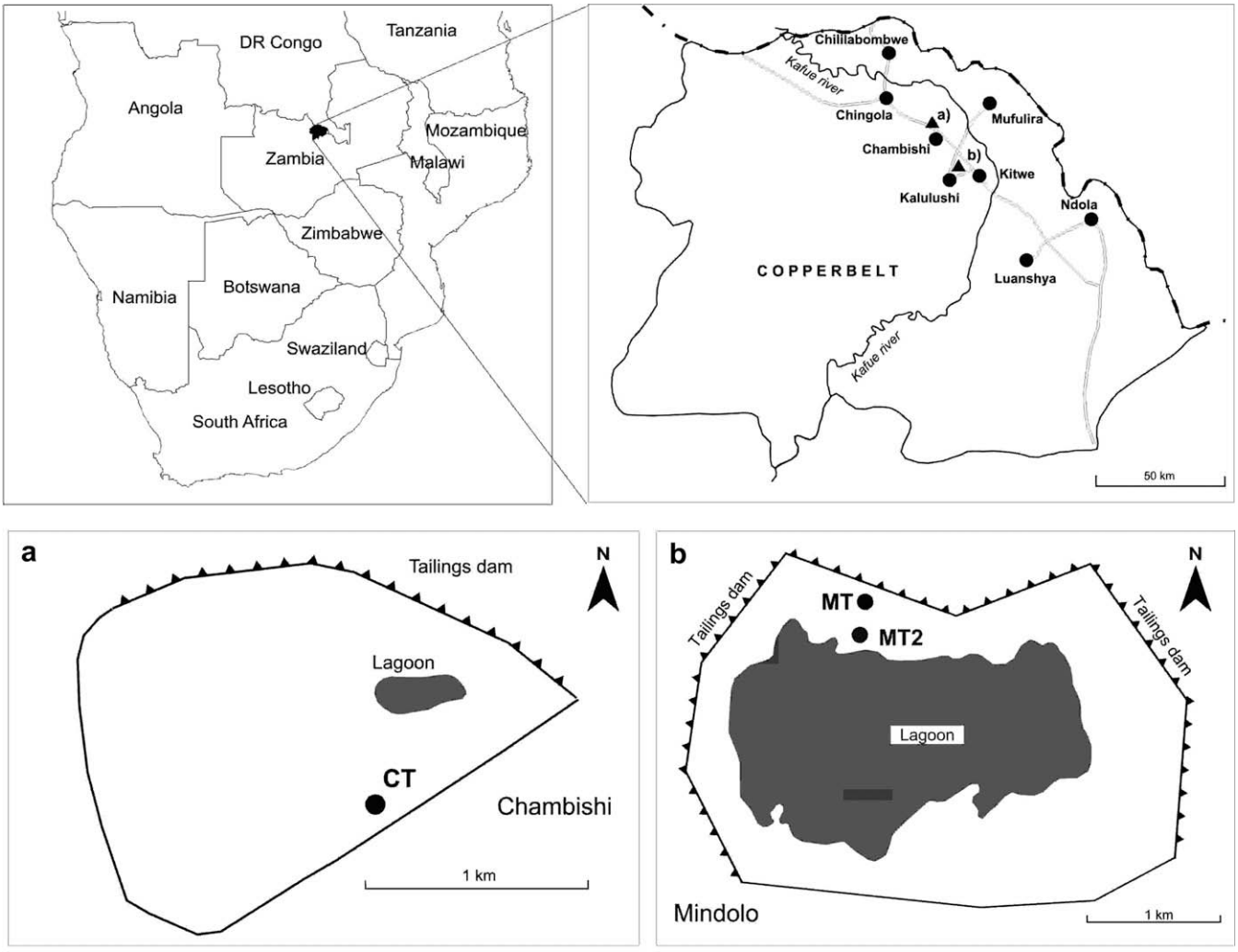

Fig. 1. Geographic location of the mine tailings sites: (a) Chambishi and (b) Mindolo.

These mine tailings comprise flotation residuals from two ore deposits. The Chambishi ore deposit, opened in the past by an open pit is now owned by Non Ferrous Metals (NFC) Africa Mining Plc. Underground mined ore is processed at the Chambishi processing plant, flotation tailings are transported by a pipe to the dam which is located north of Chambishi. The main orebody at Chambishi is confined to an interval of argillites up to 10 m thick in the Lower Roan Group of the Katanga Supergroup and has a general dip to the south. The mineralization is predominantly in the form of sulfides chalcopyrite and bornite, disseminated in black argillite called the Chambishi ore shale. The ore shale is a fine grained, well bedded argillite with thin interbeds of dolomite. At the contact of the ore shale with the footwall conglomerate, there is a 2 m thick schist zone developed as a result of shearing. Remobilization of the sulfide minerals is indicated by the increase in grain size and the concentration of these in quartz-carbonate veins up to several centimeter thick (Coats et al., 2001) About 15.3 million tons of ore at 2.37 wt.% total copper have been mined from the main ore body. Total copper reserves identified and inferred are 146 million tons at 2.30 wt.% total copper (Stalker, 1994).

The Nkana deposit, which is the source of tailings material at Mindolo, is mined at Nkana-South Ore Body shaft (production 1.3 million tons of ore per year), Nkana-Central Shaft (production 1.6 million tons of ore per year), Mindola I Shaft (production 2.02 million tons of ore per year), Mindola II shaft (production 3.67 million tons of ore per year), Northern Shaft (production 1.1 million tons of ore per year) and Subvertical Shaft (production 2.83 million tons per year). Nkana and Mindola ore bodies are separated by a barren rock interval. In the past, Nkana deposits were opened by two large, today abandoned, open pits. Total ore reserves identified and inferred are 80 million tons at total copper grade >2.0 wt.%. Underground mined ore is processed at

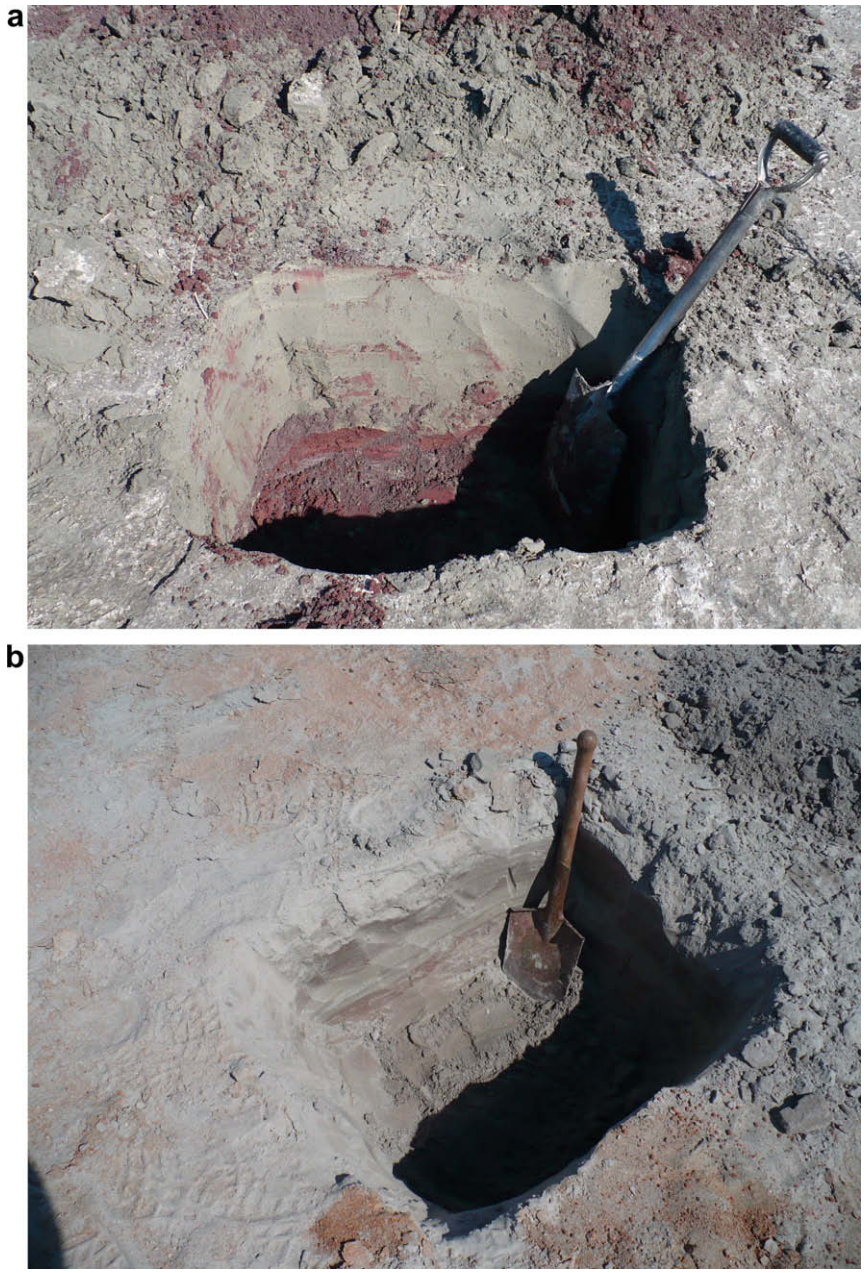

Fig. 2. (a) Old mine tailings (ca. 40 y) at Chambishi and (b) recent mine tailings (less than 10 y) at Mindolo.

Nkana Processing Plant; flotation tailings are transported by pipe to the Mindolo Dam, which is located west of Kitwe. Besides a classical underground mining, an underground acid leaching is carried out at Nkana-South Ore Body (SOB). The ore for Nkana ore body consists of (i) stratabound disseminated mineralization in black shales; (ii) stratabound massive sulfide mineralization at the boundary between black shales and underlying sandstones and conglomerates of the Mine Series (Lower Roan Subgroup) and (iii) remobilized sulfide mineralization controlled by shear zones that cut sandstones and black shales. In addition, small ore bodies occur in the Lower Conglomerate and in the Basal Quartzite. Ore is composed mostly of chalcopyrite and bornite (Coats et al., 2001).

The climate in the Copperbelt is characterized by three principal seasons: a rainy season from November to April, a dry-cold season from May to June, and a dry-hot season from August to October. The total annual precipitation is more than 1300 mm, which falls mostly during the rainy season. The principal river draining the Copperbelt mining region is the Kafue River (Fig. 1). The difference in water discharge in surface streams between the rainy and dry seasons is on the order of 100×, with a peak discharge in March and a minimum discharge in October, before the onset of rains (Petterson and Ingri, 2001).

The principal objectives of the study were: (1) to evaluate the geochemical and mineralogical transformations in mine tailings, and (2) to asses the mobility of the principal contaminants represented by copper and cobalt.

2. Material and methods

2.1. Sampling of solids and determination of physical properties

Samples of tailings solids were obtained from a hand drilling auger with an inner diameter of 4 in. The samples were preserved in polyethylene (PE) bags and later tested for bulk density and grain density, from which the air-filled porosity was calculated. The bulk density was determined on dried samples using the gravimetric technique. The grain density was measured with a Multivolume pycnometer model 1305. The samples were taken in mid-May, 2008, i.e. at the beginning of dry period.

2.2. Solid phase contents

Bulk metal concentrations were determined by X-ray fluorescence spectrometer (type ALPHA, Innov-X, Woburn, USA). Total carbon (C_{total}) and total sulfur (S_{total}) contents were determined by catalytic oxidation using a Leco elemental analyzer, sulfate sulfur ($S_{sulfate}$) content was determined by NH_4-oxalic, hot leach, and sulfide sulfur ($S_{sulfide}$) was determined from the difference. The neutralization potential ratio (NPR) was calculated on the basis

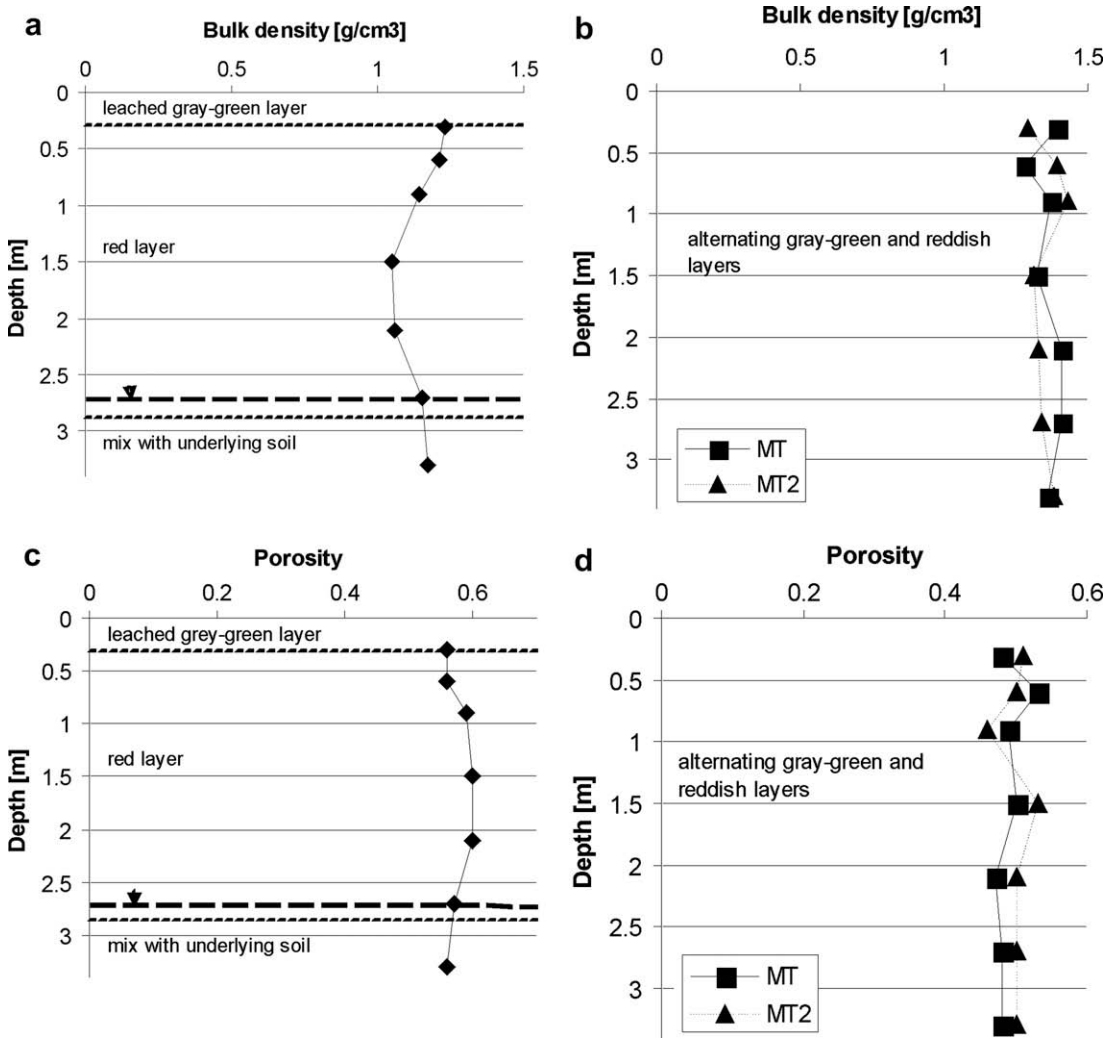

Fig. 3. Bulk density profiles at (a) Chambishi, (b) Mindolo, and porosity profiles at (c) Chambishi, (d) Mindolo; inverted triangle represents water table.

of a modified method of Sobek (Jambor, 2003), where the neutralization potential (NP) and acidity potential (AP) were calculated from C_{inorg} and $S_{sulfide}$ expressed as kg $CaCO_3$/ton of waste material, respectively.

2.3. X-ray diffraction

Selected solid phase samples were analyzed by X-ray diffraction (XRD), using a PAN-analytical X'Pert Pro diffractometer equipped with a diffracted-beam monochromator. The analyses were performed using Cu $K\alpha_1$ radiation (40 kV, 30 mA), in the range 3–80° 2θ (step size 0.02° 2θ, with a counting time of 150 s per step using X'Celerator multichannel detector). The XRD patterns were interpreted using the X'Pert HighScore software, version 1.0d (PANalytical, the Netherlands). In selected samples, the heavy minerals were concentrated by separation in bromoform ($CHBr_3$).

2.4. Electron microprobe

Several solid phase samples were also studied with an electron microprobe (EMP), using a CAMECA SX100 apparatus, equipped with five crystal spectrometers and an energy dispersive X-ray spectrum (EDS) analyzer. The wavelength dispersive X-ray spectrometry (WDS) analyses were performed at an accelerating voltage of 15 kV, a probe current of 10–20 nA, spot size 0 (oxides) to 5 μm (sulfates), a counting time 10–30 s, with natural and synthetic standards, using the PAP correction procedure.

2.5. Sequential extraction

Sequential extraction for selected samples was performed using the BCR procedure (Rauret et al., 1999). The following extraction scheme was used: a 0.11 M acetic acid (CH_3COOH) step targeting exchangeable and acid soluble fraction, a 0.5 M hydroxylamine–chloride ($NH_2OH{\cdot}HCl$) step targeting reducible fraction (mostly poorly crystalline iron/manganese oxides), an oxidisable step (8.8 M H_2O_2/1 M CH_3COONH_4 extractable) targeting organic matter and sulfides, and an Aqua Regia step targeting the residual fraction. A detailed experimental scheme is given elsewhere (Rauret et al., 1999).

2.6. Leaching tests

Paste pH was determined by equilibration of 50 g solid samples with 50 ml of deionised water. Since no water (except for one sample from the base of the Chambishi profile) was recovered from mine tailings, 50 g of homogenized sample were suspended in 150 ml of deionized water and agitated on a rotary shaker until

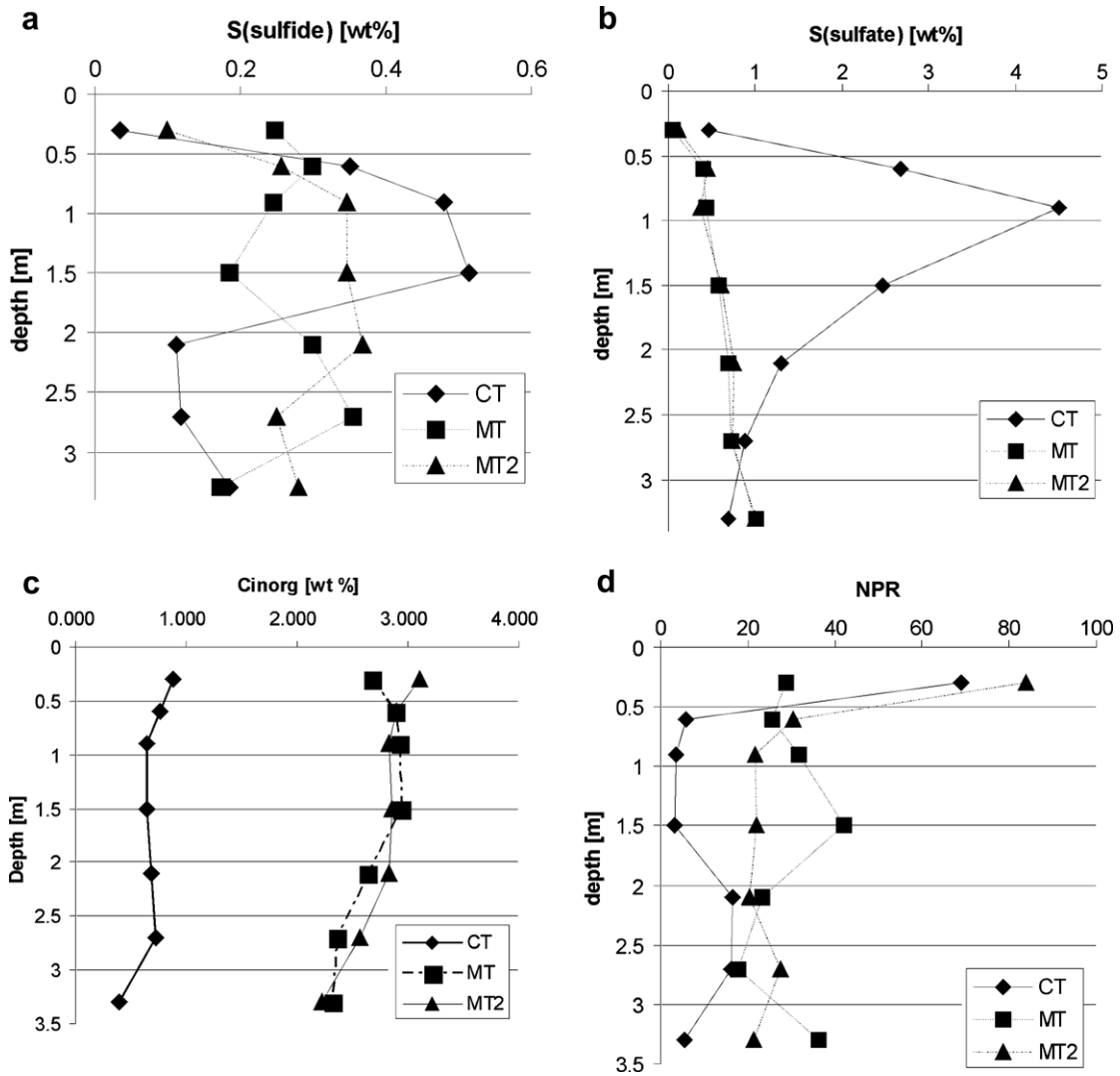

Fig. 4. Selected solid phase contents and parameters: (a) sulfidic S, (b) sulfate S, (c) inorganic C and (d) neutralization potential ratio NPR.

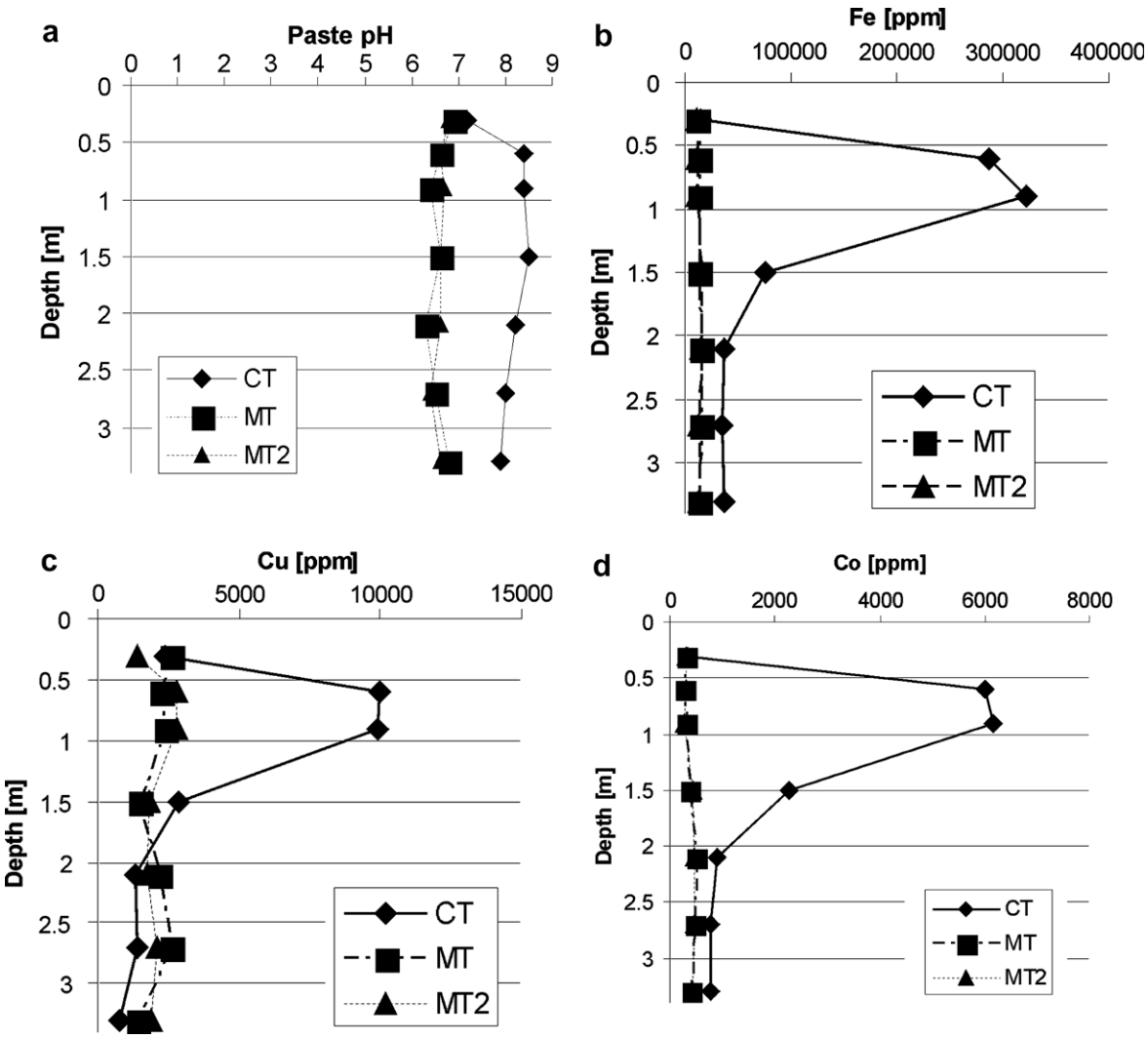

Fig. 5. Solid phase parameters and contents: (a) paste pH, (b) Fe, (c) Cu and (d) Co.

stable readings of pH and electrical conductivity (EC) were obtained. A similar approach was used by Lin (1997) and Romero et al. (2007). After stabilization of pH and EC, the leachate was decanted and filtered through a 0.45 μm filter and then split into one subsample acidified with ultrapure HCl for determination of cations and metals, and a second unacidified subsample. Cations and metals were determined by FAAS (Varian AA 280 FS) under standard analytical conditions. The analytical precision of the individual solution AAS analysis was below 5% relative for both Co and Cu determination. The detection limits for solution were 0.010 mg/l Co and 0.005 mg/l Cu, respectively. Standard reference materials BCR 483 (soil) and BCR 701 (sediment) were used for quality control of analytical data. The accuracy (expressed as percentage deviation from recommended values) did not exceed 10% for Cu.

Anions were determined by HPLC (Dionex ICS 2000). Alkalinity was determined by titration with HCl using the Gran plot to determine the end point. The only water sample collected at the Chambishi site was treated and analyzed as the leached samples described above.

2.7. Geochemical modeling

Speciation calculations were performed using the program Phreeqc (Parkhurst and Appelo, 1999) and thermodynamic data for Cu and Co were compiled from databases of minteq.dat and llnl.dat.

3. Results

3.1. Solid phase composition

3.1.1. Macroscopic characteristics and physical properties

At the Chambishi site, samples were collected from a borehole drilled to a depth of 3.6 m in the eastern sector of the mine tailings, about 250 m southwest from the central lagoon (Fig. 1a). Here the thickness of the mine tailings is only about 3 m, which is significantly less than the thickness closer to mine tailings dam (>20 m). The upper layer of tailings is about 0.3 m thick and has a light grey-green[1] color (Fig. 2a). This layer is continuous over a long distance from the drilling site and is underlined by dark red material, which continues down to the base of the mine tailings at a depth of about 3.3 m. At the base of the profile, there are spots of underlying soil, indicating mixing with soil material below mine tailings. There is also a layer of noticeable increased resistance to drilling at a depth from ca. 0.6 to 0.9 m, which was attributed to the presence of a cemented layer (hardpan). The water table was reached close to the base of profile at about 2.7 m depth. However, a relatively fine-grained material (estimated hydraulic conductivity based on grain size of about 1×10^{-7} m/s compared to

[1] For interpretation of color in Fig. 2, the reader is referred to the web version of this article.

Table 1
Results of X-ray diffraction analyses.

Mineral/sample	Chambishi CT	Mindolo MT, MT2
Quartz	xxx	xxx
Muscovite	xx	xx
Kaolinite	x	x
Orthoclase	x	x
Tremolite		x
Calcite	xx	xx
Dolomite		xx
Gypsum	xxx	x
Hematite	xxx	x

xxx – abundant, xx – present and x – detected.

1×10^{-6} m/s in the shallow zone) below 1.5 m depth seems to be tension-saturated (i.e. there is capillary fringe).

At the Mindolo site, two boreholes were drilled north of the central lagoon (Fig. 1b). Borehole MT was about 270 m from the lagoon and borehole MT2 was about 90 m from the lagoon. The material color is light grey-green, but there are discrete darker reddish bands (Fig. 2b). The ground water was not reached even at a maximum depth of 3.6 m. This is below the water level of the central lagoon, suggesting that the hydraulic connection is weak between the central lagoon and the surrounding mine tailings, presumably due to the presence of the low permeability layer at the bottom of the lagoon.

At both sites there were signs of surface flooding including ripple marks, etc. during the rainy period (November–April). This field work was performed in May and, thus, the water on the top of the tailings had probably recently evaporated before drilling began.

The vertical profile of bulk density at Chambishi (CT profile) is shown in Fig. 3a, while vertical profiles of bulk density at Mindolo (MT and MT2 profiles) are shown in Fig. 3b. The Chambishi profile indicates a higher bulk density in the upper 0.9 m, reaching about 1.2 g/cm^3. The bulk density then decreases to 1.05 g/cm^3 at 1.5 m depth. There is a moderate density increase with depth, where the mine tailings material is already mixed with underlying soil. At the Mindolo site, the bulk density in profiles MT and MT2 is similar, about 1.4 g/cm^3 and there are no distinct trends with depth. There is a slight decrease only in the shallow zone to 1.29 g/cm^3.

Porosity profiles are shown in Fig. 3c for the Chambishi site and in Fig. 3d for the Mindolo site. At the Chambishi site, there is slightly decreasing porosity to a value of 0.56 in the upper 0.9 m. In the deeper zone, the porosity reaches about 0.6 and decreases again to 0.56 at the base of the tailings. At the Mindolo site, the porosity values are lower, around 0.5. There is a porosity minimum of 0.47 at 0.9 m depth, while below 0.9 m, the porosity values are relatively constant.

Both bulk density and porosity suggests an early stage of hardpan formation at the Chambishi site, but not at the Mindolo site. This is consistent with the solid phase composition and mineralogical data (see below).

3.1.2. Bulk composition

The sulfide content S is shown in Fig. 4a. At Chambishi, the sulfide content is very low, being about 0.034 wt.% at 0.3 m,

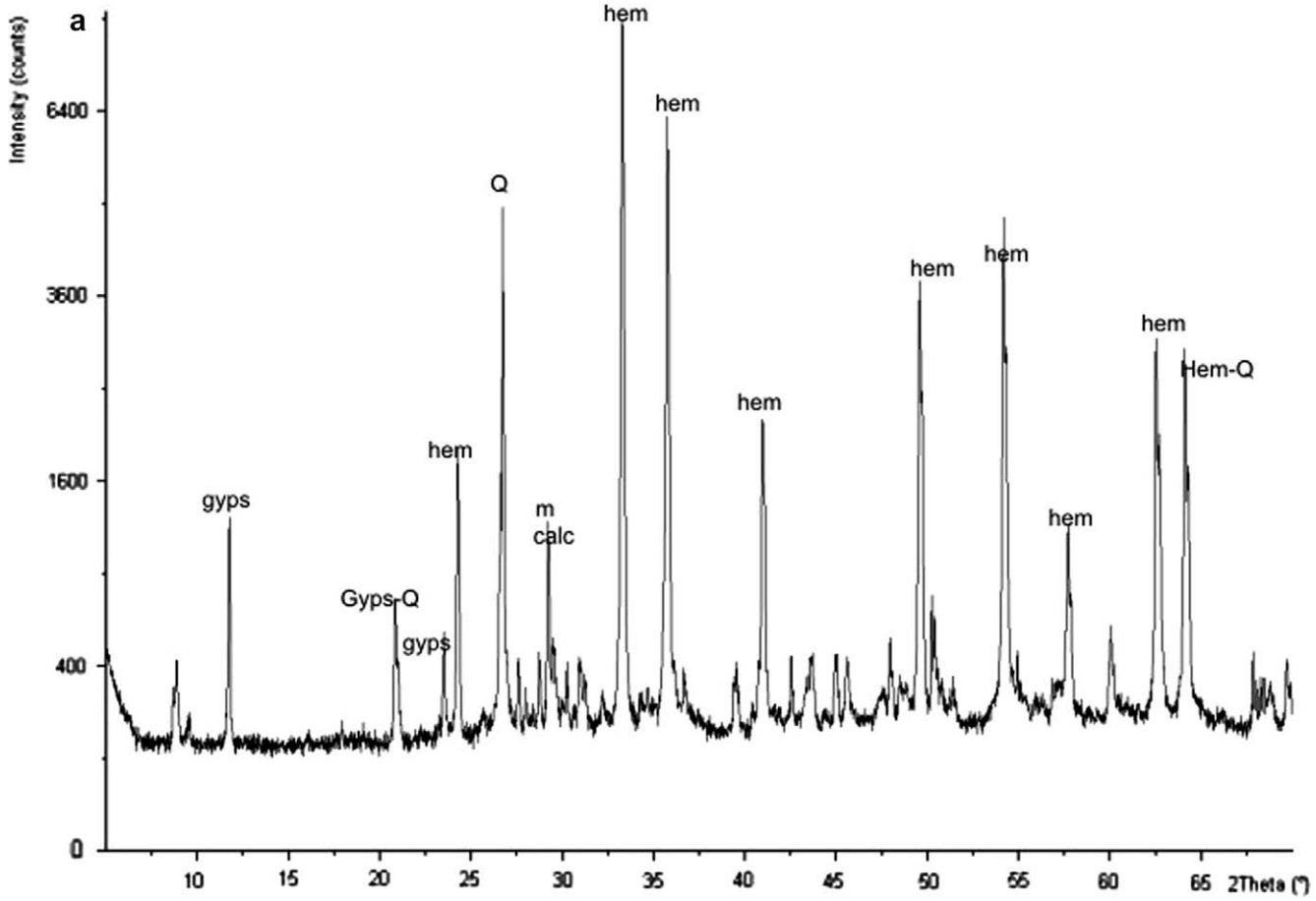

Fig. 6. Typical X-ray diffraction patterns for minerals separated in bromoform: (a) Chambishi, CT5, depth 1.5 m and (b) Mindolo, MT2, depth 0.6 m.

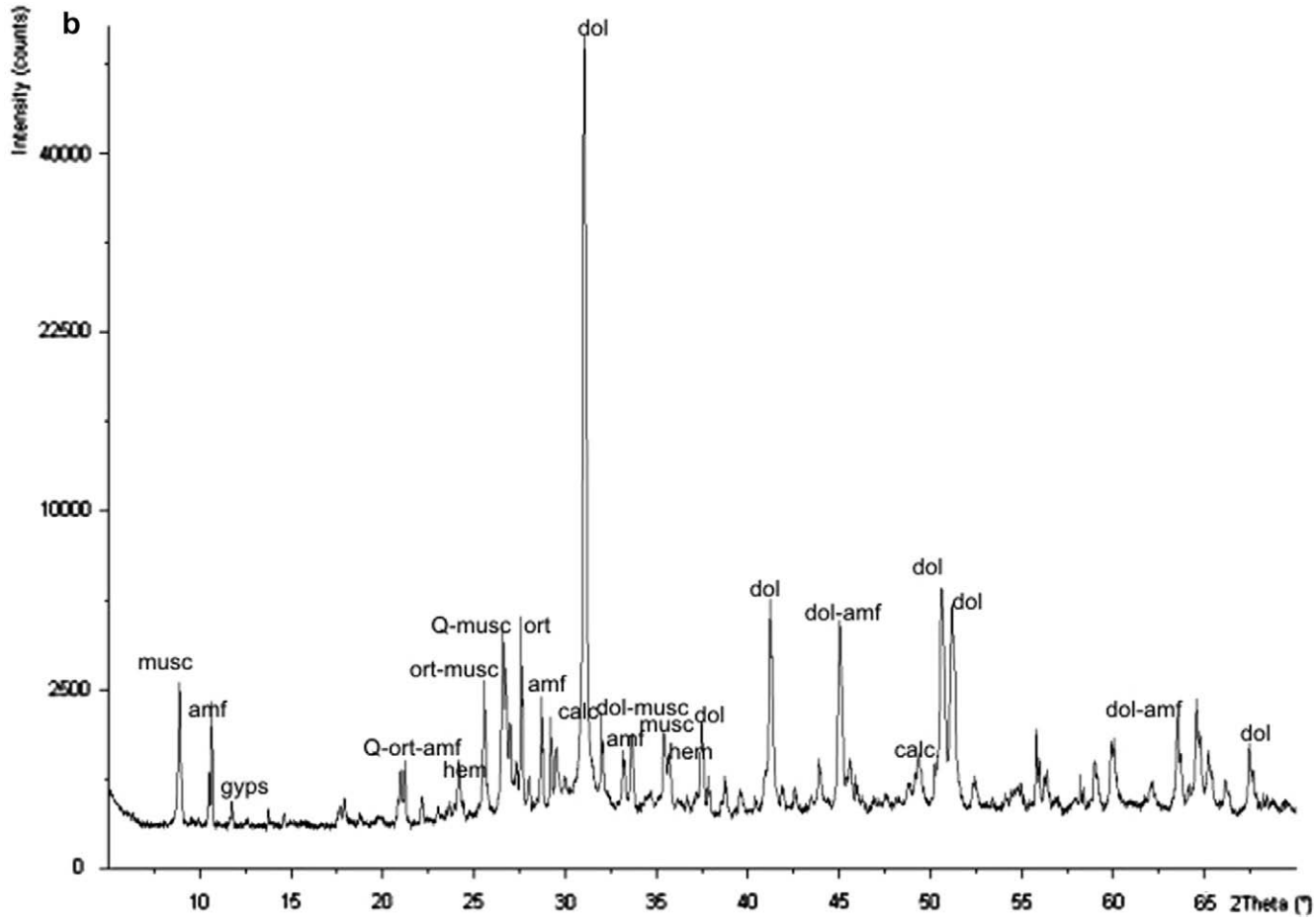

Fig. 6 (*continued*)

corresponding to a leached grey-green layer. There is a maximum sulfide content of 0.514 wt.% at 1.5 m depth and then a decreasing trend downward. At Mindolo relatively low sulfide contents are found at shallow depth (0.248 wt.% and 0.099 wt.% at profile MT and profile MT2, respectively), but increase with depth to the value of 0.367 wt.% at 2.1 m depth at profile MT2 and then decrease towards the base. Maximum sulfide contents do not reach the values observed at the Chambishi site, suggesting that the initial pyrite content was different at both sites.

The sulfate content S is shown in Fig. 4b. The most noticeable feature is an extremely high sulfate content at Chambishi of 4.49 wt.% (24.14 wt.% expressed as gypsum) at 0.9 m depth. At this profile location, the sulfate content decreases in the deep zone and reaches 0.684 wt.% (3.67 wt.% as gypsum) at the base of the tailings. At Mindolo there is a moderate increase with depth from 0.047 wt.% to 1.003 wt.% at the MT profile location and from 0.466 wt.% to 0.988 wt.%. The interpretation is complicated by the fact that sulfidic S is found in primary minerals (pyrite, chalcopyrite, etc.), but sulfate S may be transported from the place of its formation by the oxidation of pyrite, i.e. its current position indicates a maximum depth of its formation.

The inorganic carbon content C is shown in Fig. 4c. The carbon content decreases slightly with depth at the Chambishi site, from 0.88 wt.% (7.33 wt.% as calcite) at ground surface to 0.39 wt.% (3.25 wt.% as calcite) at depth. Inorganic C content in the Mindolo profiles are higher, with slightly decreasing trends downward from 2.67 wt.% (21.8 wt.% as calcite) to 2.32 wt.% (19.3 wt.% as calcite) at profile MT and from 3.11 wt.% (25.9 wt.% as calcite) to 2.22 wt.% (18.5 wt.% as calcite) at profile MT2.

The neutralization potential ratio (NPR) calculated on the basis of the adapted Sobek method is shown in Fig. 4d. At Chambishi, there is a very high value of 69 in the leached surface layer, but NPR values decrease with depth with a minimum of 3.4 at 1.5 m depth. The NPR value then increases to 16.5 at 2.1 m depth followed by a decrease towards the base of the tailings. At Mindolo, there is a very high value of 84 at profile MT2 at ground surface and 29 at the same depth at profile MT. However, the NPR values in deeper zones are always higher than 20, with a maximum of 41.9 at 1.5 m depth at profile MT. Thus, there is still a significant neutralization capacity at both sites, but at the relatively young Mindolo site, the neutralization capacity is from 2 to 7 times higher than at the older Chambishi site.

There is a difference in organic C content (not shown) between both sites, with about 0.05 wt.% at the Chambishi site and about 0.5 wt.% at the Mindolo site. There are no distinct organic C content trends with depth.

Paste pH values are provided in Fig. 5a. At Chambishi, the paste pH value is close to neutral (7.2) only in the surface layer. At 0.6 m depth, the paste pH is 8.5 and only slightly decreases to 7.9 towards the base of the profile. At Mindolo, the paste pH values are similar in both profiles with values of about 6.8 in the surface layer, then slightly decreasing with depth to about 6.5.

Total solid phase Fe content is shown in Fig. 5b. In the Chambishi profile, Fe content increases from 14,067 ppm in the surface layer to a maximum 321,614 ppm at 0.9 m depth. There is a sharp

decrease to 36,135 ppm at the base of the profile. At Mindolo, the Fe content is relatively constant and only slightly increases from about 11,000 ppm in the surface layer to about 13,200 ppm in the deeper zone.

The total solid phase Cu content is shown in Fig. 5c. In the Chambishi profile, the maximum Cu concentration corresponds to the Fe maximum, reaching 9979 ppm at 0.6 m depth and then decreasing to 795 ppm at the base. At Mindolo, the Cu content is similar, but much lower than in the Chambishi profile, with maximum values at 0.9 m depth reaching 2392 ppm and 2781 ppm in the MT and MT2 profiles, respectively, and then decreasing downward to values about 1600 ppm. Finally, the Co content is shown in Fig. 5d. All profiles are similar to the Cu profiles, but Co contents are lower. A maximum of 6175 ppm in the Chambishi profile is found at 0.9 m depth and Co contents decrease downward to values of about 790 ppm at the base. At Mindolo, the Co content is about 300 ppm in the surface layer and slightly increases to values about 420 ppm at the base of the profiles.

3.1.3. Mineralogical composition

The mineralogical composition based on X-ray diffraction of bulk samples is shown in Table 1, and typical X-ray diffraction patterns for samples separated in $CHBr_3$ are shown in Fig. 6. The principal primary minerals are quartz, muscovite, amphibole tremolite, and orthoclase. Calcite was found at both the Chambishi and Mindolo sites, but dolomite was found only at the Mindolo site. The principal difference between the sites was a much higher content of secondary gypsum and hematite (Table 1) in tailings material at the older Chambishi site compared to the younger Mindolo site. No poorly crystalline Fe(III) phases were found by X-ray diffraction at either site (Fig. 6), but were found by electron microprobe. Similarly, no primary sulfides were found by X-ray diffraction even in enriched samples, but pyrite and chalcopyrite were also found by electron microprobe.

3.1.4. Electron microprobe

Representative images of electron microprobe analyses in backscattered electron mode (BSE) for samples from Chambishi are shown in Fig. 7a,b. In Fig. 7a there are two bright Fe(III) oxyhydroxide grains in the middle and calcite grains with a characteristic cleavage above. Based on energy dispersive X-ray spectrum (EDS) analyses, the phase comprises 0.24 wt.% of Cu and 0.07 wt.% of Co. In Fig. 7b a grey quartz grain is located in the centre, surrounded by small gypsum grains, probably filling a space after dissolution of calcite. Bright coatings have Fe(III) oxyhydroxides composition with high metal contents: 6.88 wt.% of Cu and 1.89 wt.% of Co. Both samples are from 0.9 m depth with a maximum accumulation of Fe, Cu, and Co based on XRF analyses (Fig. 5).

Images of samples from Mindolo are shown in Fig. 7c,d. Here ferric iron mineral coatings are less developed. In Fig. 7c (MT profile sample from 0.6 m depth), there is a bright chalcopyrite grain in the middle with an initial stage of Fe(III) oxyhydroxide coatings, and a bright barite grain at the left. The large grain at the bottom with a characteristic cleavage is calcite. In Fig. 7d (sample from

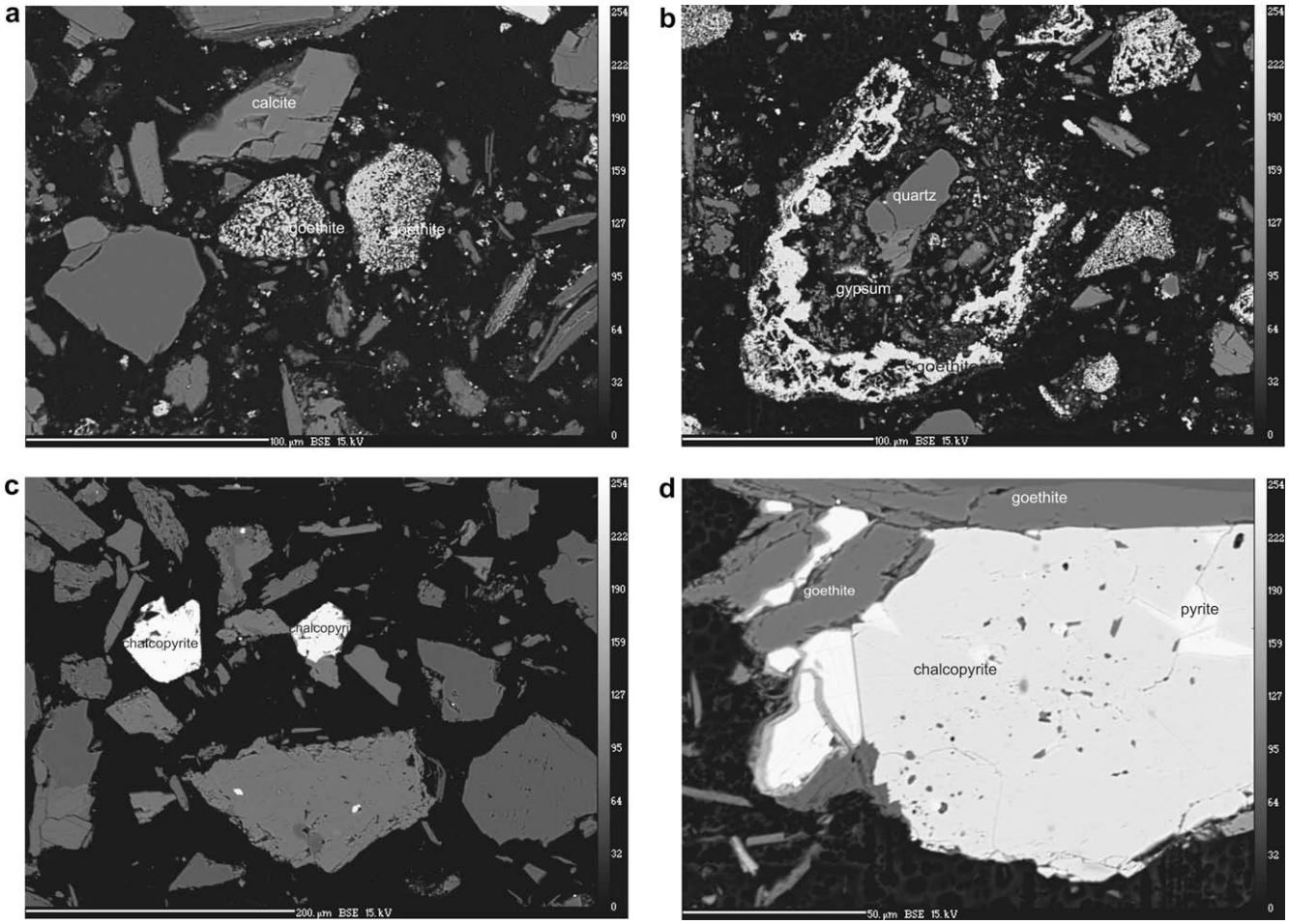

Fig. 7. Microprobe images in BSE mode: (a) sample CT3, depth 0.9 m, goethite grains in the middle, grain of calcite above, (b) sample CT3, depth 0.9 m, grain of quartz in the middle surrounded by gypsum grains covered by goethite coatings (bright color), (c) sample MT2, 0.6 m depth, bright grain at the right is chalcopyrite with initial goethite coatings, grain at the left is barite and (d) sample MT2-3, 0.9 m depth, grey grain is pyrite coated with goethite, bright spots in pyrite have chalcopyrite composition.

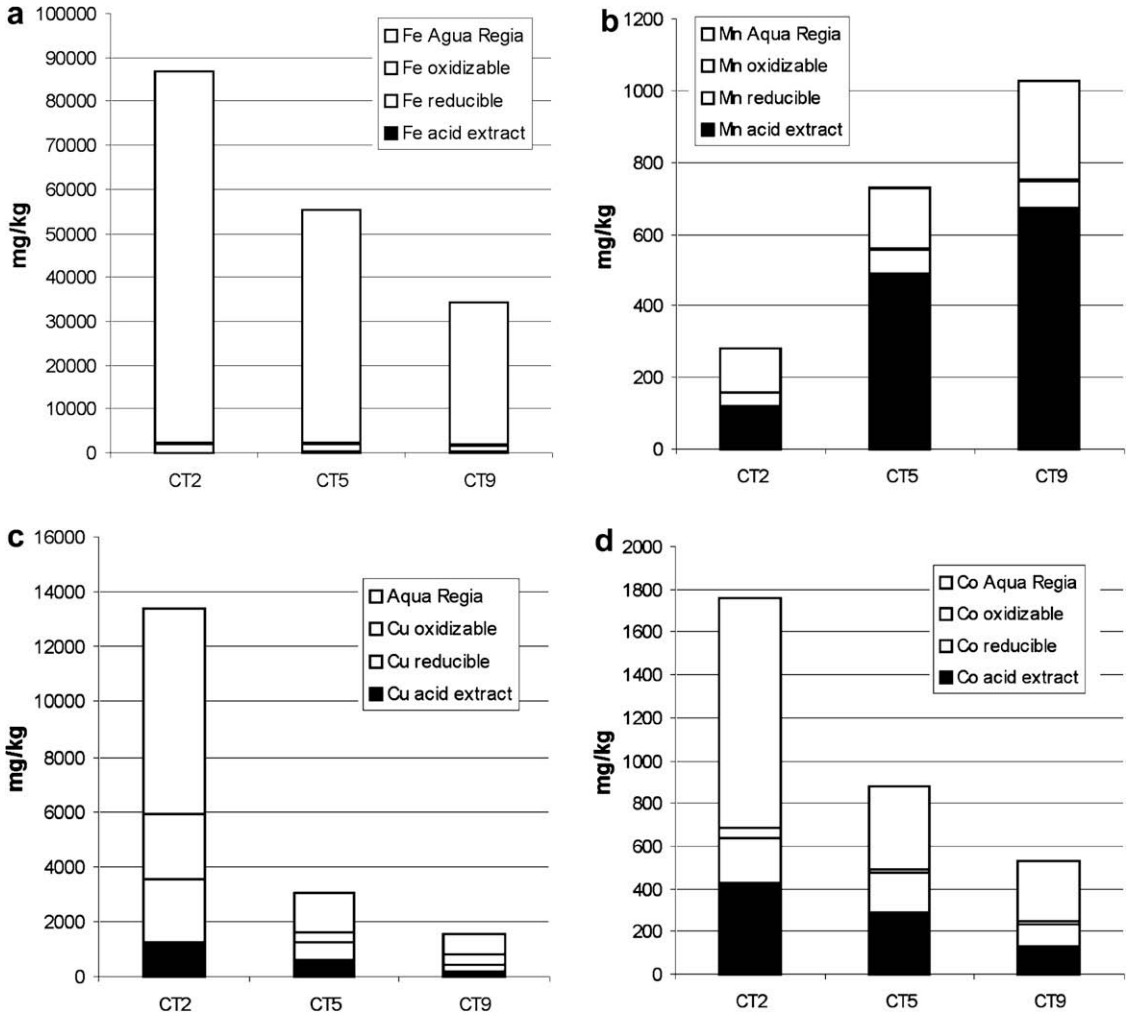

Fig. 8. Results of sequential extraction for samples from the CT profile, depths CT2-0.6 m, CT5-1.5 m, CT9-2.7 m: (a) Fe, (b) Mn, (c) Cu and (d) Co; note different scale for each graph.

MT2 profile from 0.9 m depth) a light grey pyrite grain is seen covered with dark grey Fe(III) oxyhydroxides. Brighter spots in the pyrite have a chalcopyrite composition. The Cu content in the Fe(III) phase coatings is 1.83 wt.%, while the Co content is 0.14 wt.%.

3.1.5. Sequential extraction

The solid phase content of Fe, based on sequential extraction, is shown for the Chambishi CT profile in Fig. 8a. It is evident that almost all iron (>90%) was dissolved in the Aqua Regia step and only a minor fraction in the reducible step. This suggests the presence of iron in highly crystalline phases which are very resistant to dissolution. The total content of leached Fe decreases downward, reaching a maximum of 88,000 mg/kg at 0.6 m depth. The distribution of Mn was more even (Fig. 8b), with the main fraction (>50%) dissolved in an acid extractable step and with minor fractions in the Aqua Regia and reducible steps. The trend was opposite to that of Fe, i.e., the content of extracted Mn increased downward, but the total Mn content was much lower than that of Fe, with a maximum of 1030 mg/kg, i.e., in the sample from 2.7 m depth with lowest Fe content and highest Mn content, the Fe/Mn ratio was still about 33. The trend of solid phase Cu content followed that of Fe, with a maximum content in the Aqua Regia step, but with non-negligible contents also in the reducible, oxidizable, and acid extractable steps (Fig. 8c). For Co, the highest content was in the Aqua Regia step, but the Co content in the acid extractable step was second, before the reducible and oxidizable steps (Fig. 8d). Both Cu and Co exhibited the highest contents in the sample from 0.6 m depth, which also had the highest Fe content, but the total Cu content was much higher than the total Co content (13,500 mg/kg compared to 1750 mg/kg).

At the Mindolo site, the results for MT and MT2 were similar thus only data from the MT2 profile are shown here. Solid phase Fe content is shown in Fig. 9a. Again, the highest Fe content was in the Aqua Regia step, but Fe contents in the reducible and oxidizable steps were significant, suggesting that less crystalline Fe phases are also present. The maximum Fe content of about 18,000 mg/kg was at 1.5 m depth. This is almost five times less than the maximum Fe content in the CT profile, which is closer to the surface of the tailings. The Mn content (Fig. 9b) was almost equal in the acid extractable and reducible steps, with minor contribution in the Aqua Regia and oxidizable steps. The total Mn content was similar in all samples and was higher than in the CT profile (1800 mg/kg compared to 1030 mg/kg). The total Cu content is shown in Fig. 9c. Highest Cu contents are in the acid extractable and oxidizable steps, then in the Aqua Regia step and a minimum is in the reducible step. The maximum total Cu content was located at 0.6 m depth, but the Cu content in sample MT2-9 from 2.7 m depth was also high. At this profile, the maximum Cu content was much lower than in the CT profile (3750 mg/kg compared to 13,500 mg/kg). The

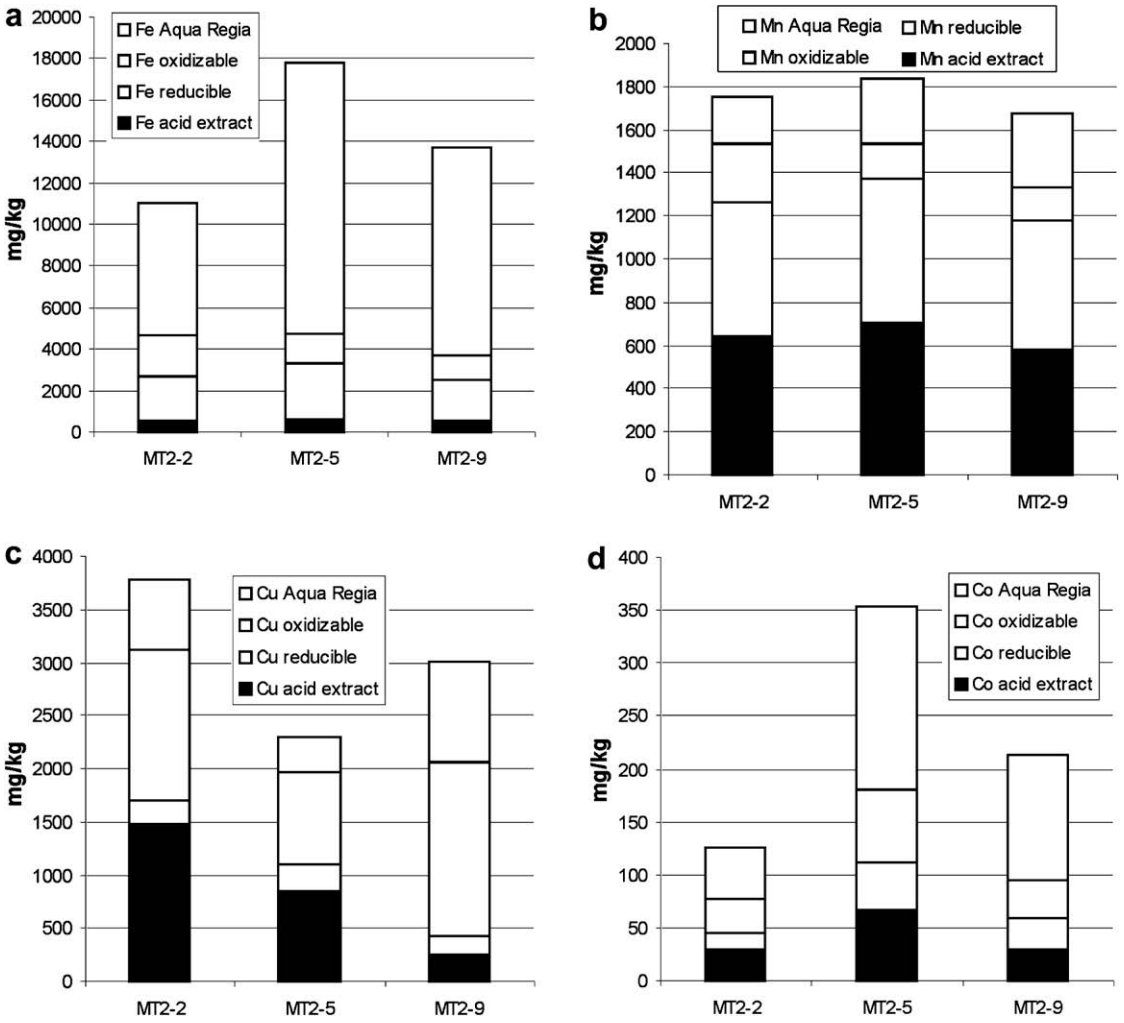

Fig. 9. Results of sequential extraction for selected samples from profile MT2, depths CT2-0.6 m, CT5-1.5 m, CT9-2.7 m: (a) Fe, (b) Mn, (c) Cu and (d) Co; note different scale for each graph.

maximum Co content was found in the Aqua Regia step (Fig. 9d) and almost equal distributions of Co were found among the remaining steps. The maximum of 355 mg/kg was located at 1.5 m depth, which is lower than the maximum of 1750 mg/kg in the CT profile. In summary, metal contents at the Mindolo site are lower than at the Chambishi site (an exception is Mn) and there are clearly defined depth trends at the Chambishi site (decreasing Fe, Cu, and Co; increasing Mn), but not at the Mindolo site.

3.2. Water chemistry

There was only one ground water sample collected at the Chambishi tailings from a depth of about 3.0 m. At the Mindolo site, both profiles down to 3.6 m were only partly saturated and for this reason sampling of ground water was impossible.

Water chemistry of the sample from the base of the Chambishi tailings is shown in Table 2.

The ground water in the Chambishi tailings has an alkaline pH of 9.5 and a moderately reducing Eh of 370 mV, indicating a post-oxic environment. The very high pH value was probably caused by a liquid junction effect due to a very high content of red suspension material in the sample. After filtration, the pH value dropped to 7.5. The dominant cation is Ca, but the concentration of K is also significant. In contrast, the Mg concentration is very low. Sulfate is a principal anion, the bicarbonate concentration is much lower and the Cl concentration is almost negligible. Concentrations of Fe and Mn are low (0.07 mg/l and 0.013 mg/l), suggesting that their concentrations are controlled by the precipitation of their mineral phases. Respective concentrations of Cu and Co are 0.006 mg/l and 0.012 mg/l.

Selected results of speciation modeling performed with pH measured on filtered sample are provided in Table 3.

Ground water is supersaturated with respect to calcite, undersaturated with respect to dolomite and is at equilibrium with respect to gypsum. There also is supersaturation with respect to Fe(III) minerals $Fe(OH)_3$(a), goethite and hematite, suggesting that these phases control the Fe concentration in solution. This is consistent with the mineralogical analyses. Ground water is also

Table 2
Chambishi: ground water chemistry, depth 3.0 m bgs, concentrations in mg/l.

Parameter	pH	Eh (mV)	Ca	Mg	Na	K	Fe	Mn	Cu	Co	SO_4	Cl	HCO_3
Sample CT	9.5, 7.5[a]	370	568	0.67	45	353	0.07	0.013	0.006	0.012	1820	5	71.4

[a] Measured on filtered sample, see explanation in text.

Table 3
Chambishi: selected results of pore water speciation modeling.

SI value	Calcite	Dolomite	Gypsum	$Fe(OH)_3(a)$	Goethite	Malachite	MnOOH	$Co(OH)_2$	$CoCO_3$
Sample CT	**0.24**	−2.12	**0.00**	**2.72**	**7.52**	−1.53	−3.73	−5.81	−3.02

Bold – supersaturation.

undersaturated with respect to manganite, MnOOH and rhodochrosite, $MnCO_3$. However, this has to be interpreted with caution because total Mn and Fe concentrations were split on the basis of Eh, i.e., a redox equilibrium was assumed. Saturation with potential secondary Cu and Co mineral phases like malachite, $Cu_2CO_3(OH)_2$, and sphaerocobaltite, $CoCO_3$, is not reached which indicates that adsorption on or co-precipitation with Fe(III) and Mn(IV) minerals might be a mechanism controlling their dissolved concentrations. There is strong undersaturation with respect to Cu and Co sulfides. The principal dissolved species of copper is $Cu(OH)_2^0$ (84.7%), other species are Cu^{2+} (8.4%) and $Cu(SO)_4^0$ (5.1%). Speciation of cobalt is dominated by Co^{2+} (62.3%) followed by $CoSO_4^0$ (34.3%).

3.3. Leaching tests

Results of water leaching tests for principal cations are shown in Fig. 10. Calcium completely dominates in all profiles, reaching concentration of 625 mg/l at 0.9 m in the CT profile and only slightly drops to 590 mg/l in the deepest sample (Fig. 10a). In the MT profile, only the sample at 0.3 m depth has a low concentration of Ca (33 mg/l), but deeper samples have concentrations in the range from 560 to 600 mg/l (Fig. 10b). The situation is similar in the MT2 profile, where Ca concentrations range from 572 mg/l to 613 mg/l with a maximum at 1.5 m depth (Fig. 10c). Other cations have much lower concentrations, with potassium in the range from 33 mg/l to 51 mg/l at all profiles. Concentrations of Na are generally below 10 mg/l, and concentrations of Mg are below 20 mg/l. Concentrations of Mg are especially low in the CT profile with a maximum of 2.7 mg/l. In the MT and MT2 profiles, Mg concentrations reach 20 mg/l in some samples.

Concentrations of leached anions are shown in Fig. 11. Chlorides were omitted because their concentrations are <5 mg/l. Sulfate dominates in all profiles, typically in the range from 1300 mg/l to 1480 mg/l. The only exception is in the shallowest sample of the MT profile with a sulfate concentration of 61 mg/l. Concentrations of bicarbonate are much lower, in the range from 48 mg/l to 70 mg/l in all profiles. There is no significant difference between profile CT (Fig. 11a), where carbonates were partly depleted, and profiles MT (Fig. 11b) and MT2 (Fig. 11c) with relatively fresh tailings material.

Concentrations of leached metals are shown in Fig. 12. In the CT profile (Fig. 12a), the maximum concentration of Fe is 1.24 mg/l at 0.6 m depth and then drops to about 0.4 mg/l except in the deepest

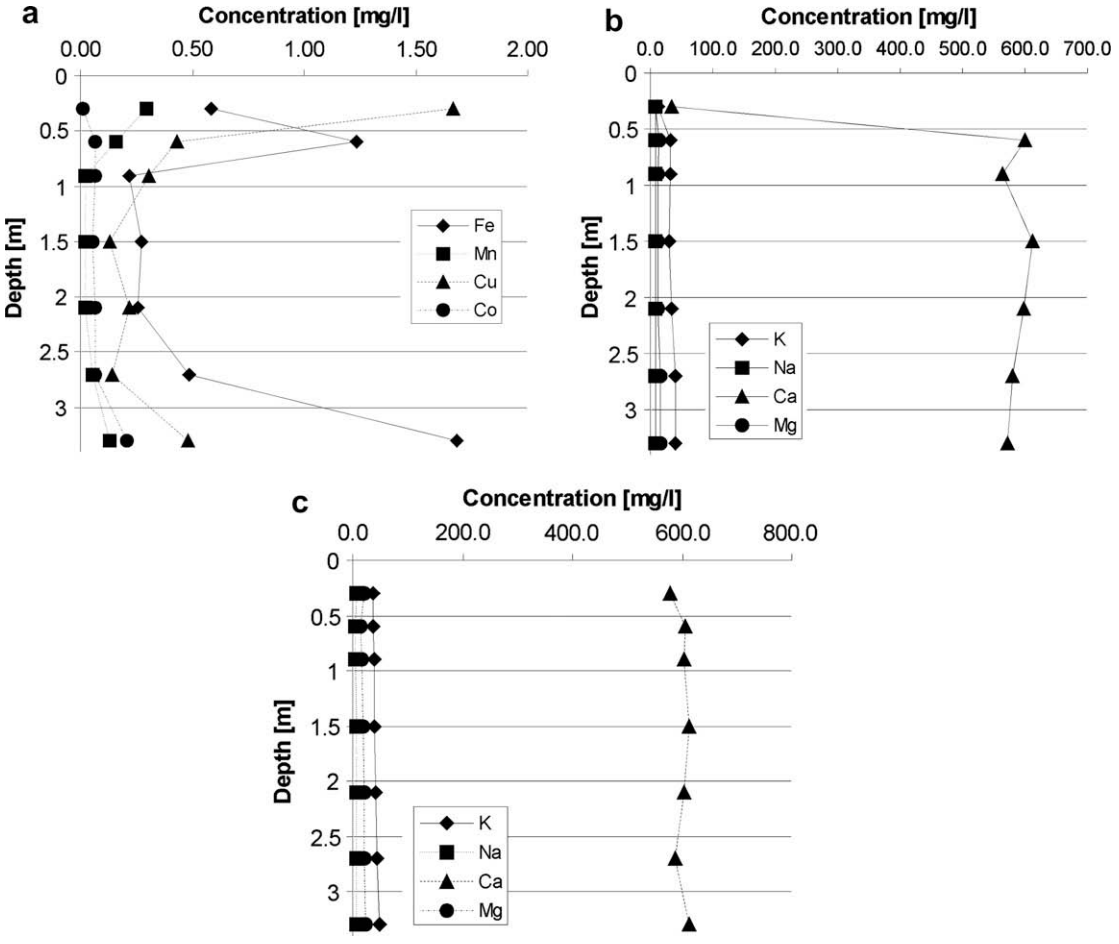

Fig. 10. Results of solid phase leaching: cations – (a) CT, (b) MT and (c) MT2.

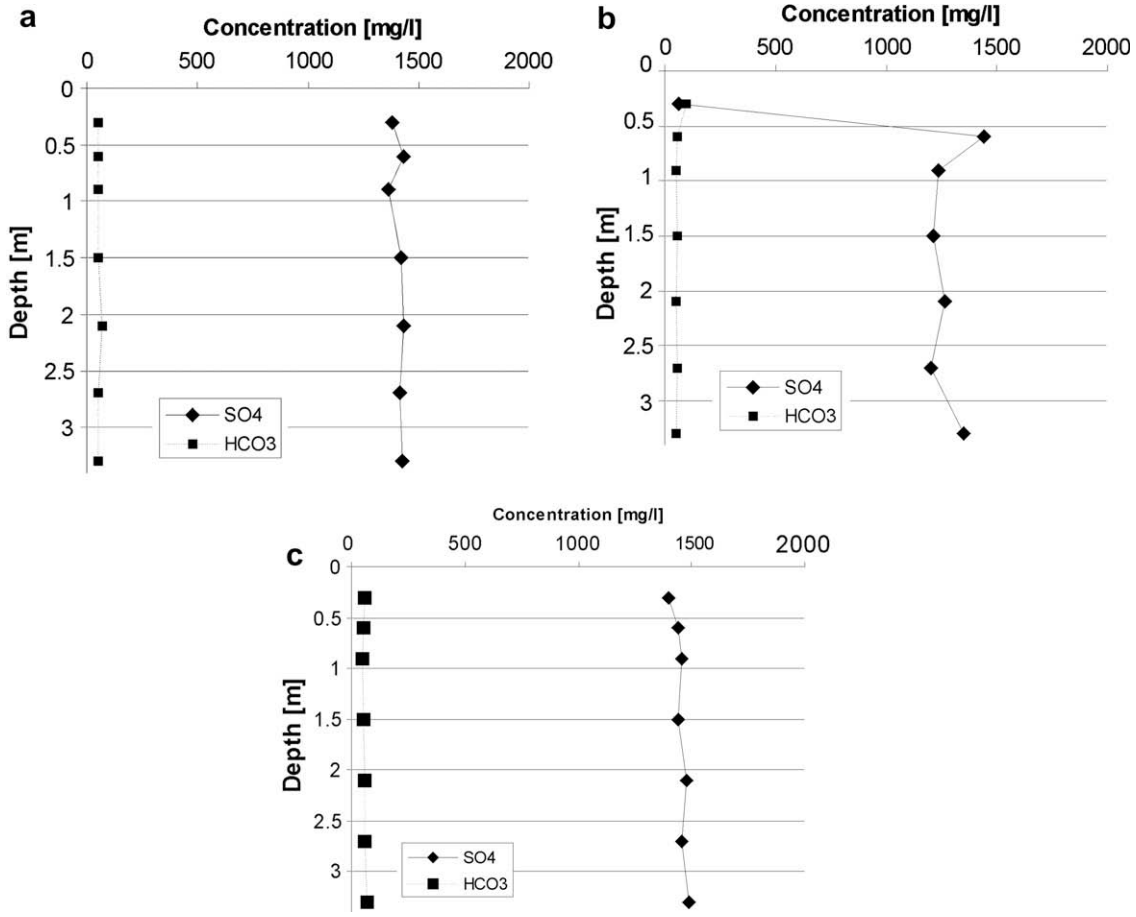

Fig. 11. Results of solid phase leaching: anions – (a) CT, (b) MT and (c) MT2.

sample with concentrations of 1.63 mg/l. Concentrations of Mn are much lower than those of Fe, below 0.3 mg/l. The Cu concentration profile resembles the Fe profile, with a maximum 1.67 mg/l in the shallowest sample. Concentrations of Co are much lower, below 0.2 mg/l. In the MT profile (Fig. 12b), Fe concentrations reach a maximum of 2.0 mg/l at 0.3 m depth, then decrease to 0.7 mg/l and increase again close to the base of the profile. Concentrations of Mn are again lower than concentrations of Fe and increase towards the base of the profile to values of about 0.6 mg/l. Cu concentrations closely follow those of Fe, but they are slightly lower, with a maximum of 1.26 mg/l in the shallowest sample. Concentrations of Co are lower, and increase downward with a maximum of 0.358 mg/l at 2.1 m depth. Finally, the MT2 profile (Fig. 12c) is similar to the MT profile, with Fe and Cu concentrations closely linked. Maximum concentrations of Cu and Fe are found at 0.6 m depth, with values of 3.0 mg/l and 2.63 mg/l, respectively. Mn and Co concentrations are lower, with similar trends for both metals and maximum concentrations at 2.1 m depth.

Saturation indices for selected minerals based on leaching tests are shown in Fig. 13. All samples except the sample from the top of the MT profile (Fig. 13b) are at or close to equilibrium with respect to gypsum, suggesting that this phase controls the concentration of Ca and sulfate in water. Also, all samples are supersaturated with respect to amorphous $Fe(OH)_3(a)$. Saturation indices for goethite and hematite (not shown) are from 7.0 to 8.0 and from 17 to 19, respectively. All samples are undersaturated with respect to calcite and manganite, MnOOH. Shallow samples from Mindolo (profiles MT and MT2) are supersaturated with respect to secondary Cu minerals brochantite, $Cu_4(SO_4)(OH)_6$, and malachite, $Cu_2CO_3(OH)_2$ (Fig. 13b and c), but samples from Chambishi (Fig. 13a) are undersaturated with respect to these phases. However, saturation is not reached with respect to any mineral phase of Co such as sphaerocobaltite, $CoCO_3$, and $Co(OH)_2$ (not shown).

4. Discussion

In mine tailings, the process generating mine drainage is the oxidation of sulfides like pyrite (Blowes et al., 2003),

$$FeS_2(s) + 3.5O_2(g) + H_2O = Fe^{2+} + 2SO_4^{2-} + 2H^+ \quad (1)$$

When fast-acting neutralization minerals like calcite are present in the solid phase, they neutralize acidity produced by the oxidation of pyrite and gypsum precipitates simultaneously,

$$CaCO_3(s) + 2H^+ + SO_4^{2-} + 2H_2O = CaSO_4 \cdot 2H_2O(s) + H_2CO_3 \quad (2)$$

In the unsaturated zone of mine tailings, Fe^{2+} is oxidized to Fe^{3+} and, under relatively high pH conditions, there is precipitation of ferric hydroxides,

$$FeS_2(s) + 3.75O_2(g) + 3.5H_2O = Fe(OH)_3(s) + 2SO_4^{2-} + 4H^+ \quad (3)$$

These processes result in close to neutral pH water with high concentration of Ca and sulfate, but low concentrations of iron. Ferric oxide and hydroxides also are efficient adsorbents of metals like Cu and Co. When chalcopyrite is oxidized, initially there is no production of acidity, which is produced by hydrolysis of iron and precipitation of ferric hydroxide later,

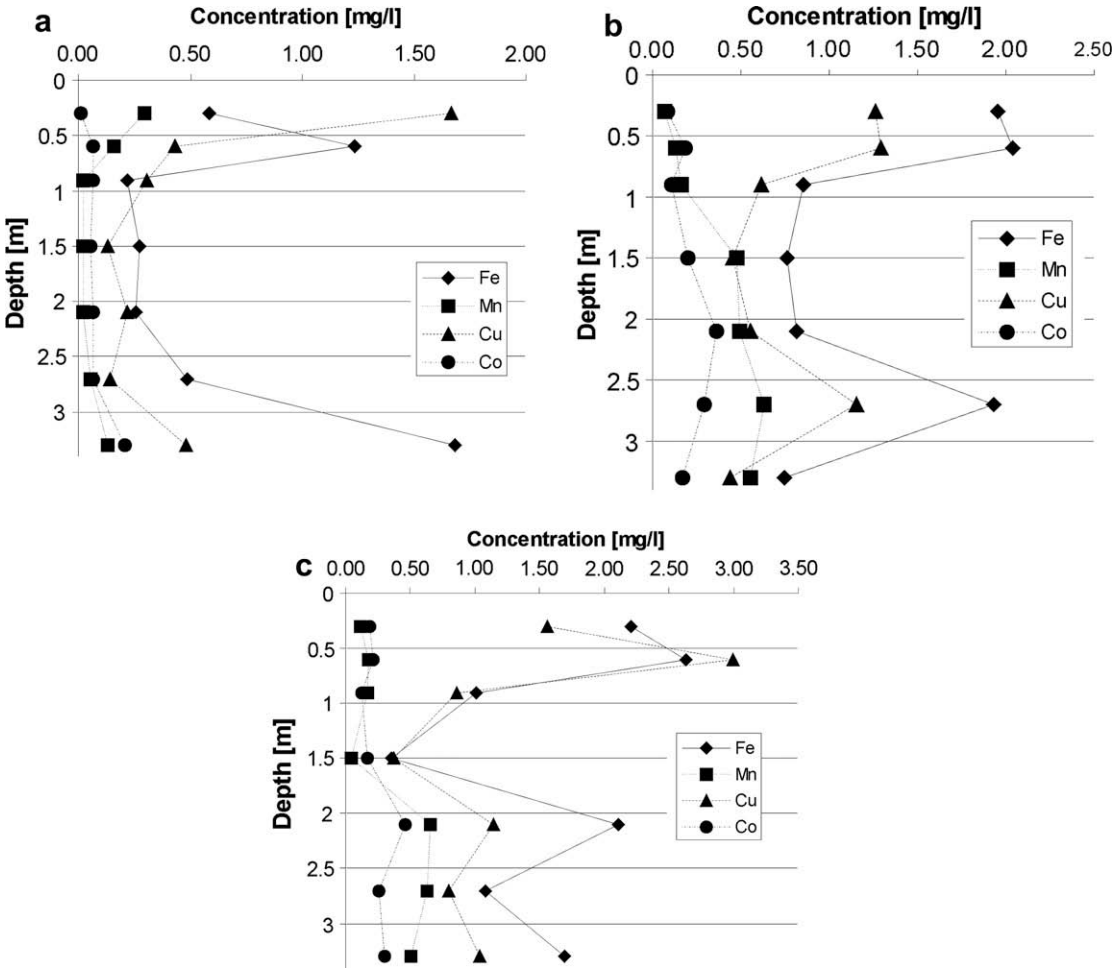

Fig. 12. Results of solid phase leaching: metals – (a) CT, (b) MT and (c) MT2.

$$CuFeS_2(s) + 4.25O_2(g) + 2.5H_2O = Fe(OH)_3(s) + Cu^{2+} + 2SO_4^{2-} + 2H^+ \quad (4)$$

The second most important cation in water is potassium, which is probably released by the dissolution of orthoclase,

$$2KAlSi_3O_8(s) + 2H^+ + 9H_2O = 2K^+ + 4H_4SiO_4^0 + Al_2Si_2O_5(OH)_4(s) \quad (5)$$

This reaction is incongruent, also consumes acidity and results in the formation of kaolinite. There also are non-negligible concentrations of Mg in leachate samples from the Mindolo site. Mg is probably released by the dissolution of dolomite, which was found by X-ray diffraction.

As evident from the equations above, pyrite oxidation coupled to the precipitation of ferric hydroxide produces two times more acidity than the oxidation of chalcopyrite coupled to the precipitation of ferric hydroxide. At the Chambishi and Mindolo sites, several types of sulfides including pyrite and chalcopyrite are present. However, the neutralization capacity of the tailings material at the Chambishi site is still high even after about 40 y and the neutralization potential ratio (NPR) is about 3.4 at shallow depths and 16.5 in the deeper zones. This is consistent with high carbonate contents (above 7.0 wt.% as calcite) and high paste pH values. At the Mindolo site, the NPR values are typically >20. Thus, at both sites acidity is consumed completely and the pH remains neutral. This results in low concentrations of Fe(III) in pore water and, thus, in relatively low pyrite oxidation rate because ferric iron is a strong oxidant (Blowes et al., 2003). Also, ferric minerals produced in both reactions cover the surface of sulfide grains, thus decreasing the sulfide oxidation rate (Nicholson et al., 1990). At the Chambishi site, ferrihydrite formed in early stages of neutralization is later transformed to hematite, which is very resistant to weathering.

Due to the neutral character of the mine tailings material, there was formation of initial hardpan composed of gypsum and ferric mineral phases like hematite at the older Chambishi site. At the relatively young Mindolo site, no cemented zone is observed. When mine tailings contain carbonates, there is formation of gypsum hardpan at the early stages, which is transformed to jarosite hardpan later, after depletion of carbonates (McGregor and Blowes, 2002). Stability of gypsum requires the presence of calcium in pore water, which is provided by the dissolution of carbonates like calcite. Gypsum and jarosite may co-exist, but gypsum is already dissolving at this stage (Sracek et al., 2004). Transformation of poorly crystalline phases like ferrihydrite to more crystalline phases like goethite and hematite decreases the surface area available for adsorption of metals. This may cause release of previously adsorbed and co-precipitated metals (Langmuir, 1997, Lottermoser and Ashley, 2006). However, once hematite is formed, it is very resistant to dissolution and iron and incorporated metals are very immobile (Dokoupilová et al., 2007). This is in good agreement with low pore water concentrations of Cu and Co (Table 2). At the Chambishi site there still is a gypsum stage of hardpan formation, which will continue until the neutralization capacity of the mine tailings material is depleted. At the relatively recent Mindolo site there has not been any formation of hardpan so far. The pres-

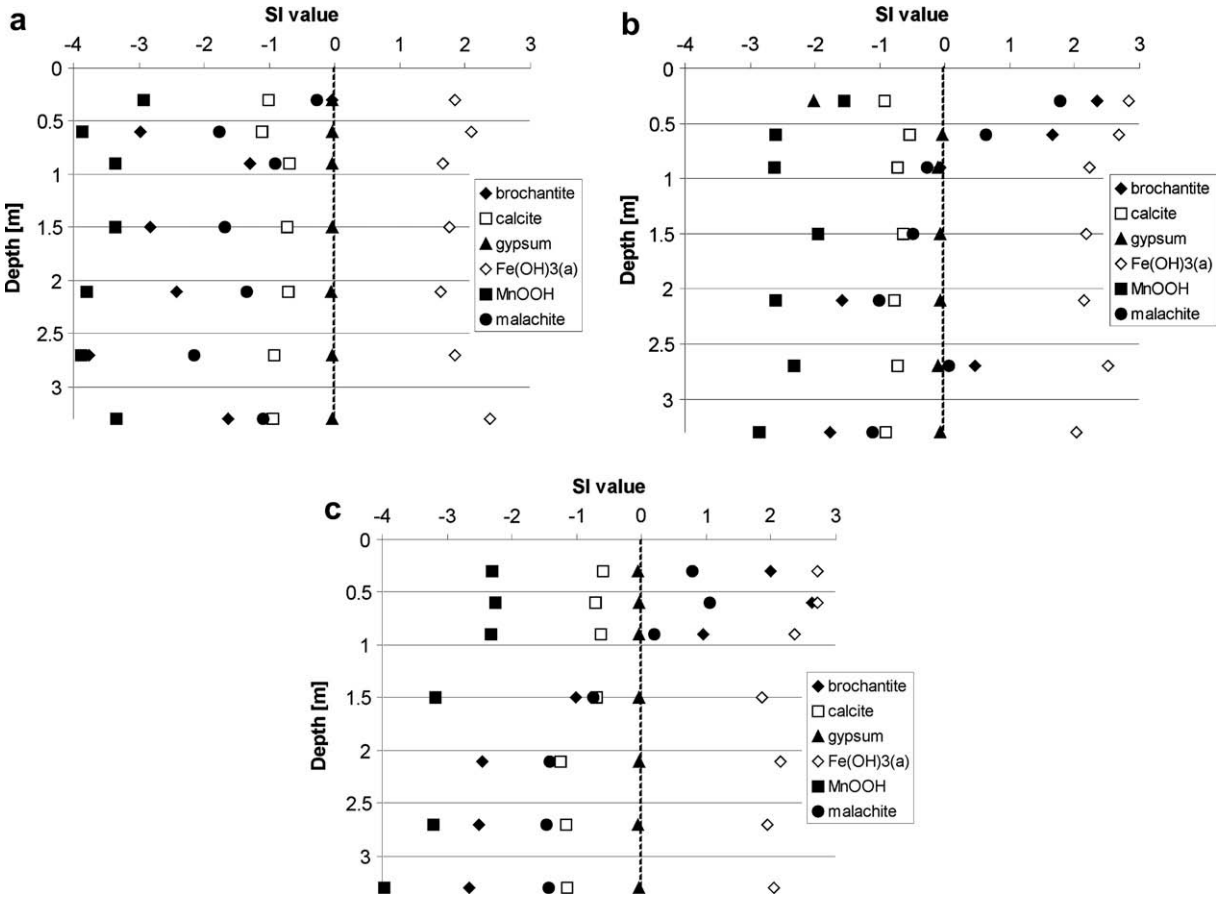

Fig. 13. Leaching tests, SI values for selected minerals, dotted line indicates equilibrium: (a) Chambishi CT, (b) Mindolo MT and (c) Mindolo MT2.

ence of hematite in hardpan at Chambishi indicates advanced stage of ferric minerals aging. However, hematite is also present at the much younger Mindolo site, albeit its content is lower. Hematite is typically formed in warm climate soils and is the chief oxyhydroxide in red-bed sediments (Langmuir, 1997). The increasing Mn content with depth (Fig. 8b) might be explained by co-precipitation of Mn with carbonates like calcite because saturation with respect to rhodochrosite was not reached. There is also more Co than Cu released in the acid extraction step (Fig. 8c and d). This may be caused by the precipitation of (Ca, Co)-carbonate solid solution on the surface of calcite (Xu et al., 1996).

In leaching tests, Cu seems to mimic the behavior of Fe, but Co follows the behavior of Mn (for example, Fig. 12b). This may be caused by the release of Cu adsorbed on or co-precipitated with Fe(III) minerals and the release of Co from the surface of Mn-rich calcite.

Saturation index values indicate a possibility of secondary Cu mineral precipitation including brochantite, $Cu_4(SO_4)(OH)_6$, and malachite, $Cu_2CO_3(OH)_2$, at shallow depths of the Mindolo site (Fig. 13b and c). It is not clear, however, if this is caused by the dissolution of Tertiary minerals in the terminology of Jambor (1994), (i.e. minerals, which precipitated after sampling). It seems that these phases had already been present in the mine tailings before sampling because the mass water/solid ratio was 3:1 in leaching experiments, but the same ratio (assuming bulk density of 1.5 kg/dm^3 and porosity of 0.4) is at least 1:3.75 and perhaps as low as 1:30 for relatively dry surface tailings samples. This suggests that the magnitude of supersaturation was much higher in the field. Precipitation of secondary Cu-sulfate minerals was found at porphyry copper ore tailings deposited in Chile in arid climate conditions by Dold and Fontboté (2001). However, conditions at these Chilean mine tailings are much more acidic than in the Zambian mine tailings and, thus, precipitation of carbonate minerals like malachite is therefore impossible.

The red color down to a depth of about 3.3 m at the Chambishi site is surprising because the typical depth of sulfide oxidation in moderate climates, even in old mine tailings, is 1.5–1.8 m (McGregor et al., 1998; Moncur et al., 2005). A possible explanation is in the large changes of redox conditions between the rainy and dry season. The Copperbelt experiences a high precipitation of about 1300 mm per year, which falls only during the rainy period from November to April. During our sampling in May there were visible signs of previous water ponding on the surface of the tailings. Thus, ferric iron minerals which precipitate during dry periods close to tailings surface may dissolve under temporarily reducing conditions and the ferrous iron will be transported downward by infiltrating water. When the tailings dry up during the dry period from May to October, the conditions become oxidizing again and ferric minerals precipitate at higher depths than the depth of the sulfide oxidation front.

Another puzzling feature is a sharp interface between the shallow grey-green layer on the top of the profile at Chambishi, which is from 0.2 m to 0.4 m thick, and a red layer located underneath (Fig. 2a). The layer is located on the top of the cemented layer comprising gypsum and hematite at a depth 0.6–0.9 m. No such layer is observed at the Mindolo site. There are two possible explanations for the thin grey-green layer found at the Chambishi site: (a) this layer represents material which was deposited at mine tailings after a relatively long break in sedimentation, and, thus, there was not enough time for sulfide oxidation and precipitation of Fe(III) minerals, and (b) this layer is a consequence of intense leaching of the upper layer, which was originally also rich in ferric

oxyhydroxides. Explanation (b) seems to be more probable because there is very low $S_{sulfide}$ content (0.03 wt.% compared to 0.36 wt.% in red material from 0.6 m depth), (Fig. 4a), and low Fe content (Fig. 5b) in the grey-green surface layer. Unfortunately, no information about the history of mine tailings at Chambishi is available because the site changed owner after deposition of the mine tailings.

Our results are consistent with those obtained by von der Heyden and New (2004) at mine tailings south of our study site. They also found relatively low concentrations of dissolved metals and neutral pH conditions caused by high neutralization capacity in mine tailings impoundment. However, they admitted a possibility of acid mine drainage at some sites in the Copperbelt.

5. Conclusions

Two sulfidic mine tailings at the Zambian Copperbelt in the north of Zambia have been investigated: Chambishi, representing an older site (about 40 y) and Mindolo, which represents a relatively recent site (less than 10 y). Maximum solid phase sulfide S contents are 0.514 wt.% at Chambishi site and 0.367 wt.% at Mindolo site. They are much lower than respective maximum inorganic C contents 0.88 wt.% and 3.11 wt.%. The neutralization capacity based on solid phase carbonates remains high and neutral to alkaline conditions predominate at both sites. The principal secondary minerals at both sites are gypsum, and Fe(III) phases like amorphous oxyhydroxides and hematite. Amorphous Fe(III) phases form coatings on the surface of primary sulfides like pyrite and chalcopyrite and incorporate large quantities of copper and cobalt in the surface rims (up to 7.0 wt.% of Cu and up to 2.0 wt.% of Co). At the Mindolo site, there seems to be precipitation of secondary Cu minerals such as brochantite and malachite in the zone of evaporation enrichment close to the surface of the mine tailings.

High Fe(III) phases content results in a red staining of the mine tailings material, which is evident even below the assumed depth of the pyrite oxidation front. This can be explained by reductive dissolution of Fe(III) phases under temporarily reducing conditions during the rainy period, when dissolved iron is transported by infiltrating water to the deeper zone of the mine tailings, where it reprecipitates later. At the Chambishi site, precipitation of secondary minerals resulted in an early stage of hardpan formation at 0.6–0.9 m depth, formed mostly by gypsum and hematite. This zone also corresponds to maximum Cu and Co contents. The presence of hematite results in low solubility of iron in all sequential extraction steps except the Aqua Regia step. Concentrations of Ca and sulfate are controlled by equilibrium with gypsum. At this site, there is a 30-cm thick grey-green surface layer with low sulfide content, probably formed as a consequence of intense leaching during the rainy season.

No hardpan was found at the more recent Mindolo site, where the red tailings material is present only in discrete band zones. Hematite and gypsum are also present, but in lower amounts. Most of Fe and Co is dissolved in the Aqua Regia step, but Mn and Cu are distributed more equally. At this site, formation of hardpan may be expected in later stages of the mine tailings evolution.

Regarding the remaining neutralization capacity, there does not seem to be a threat of acid mine drainage for at least a few decades. Also, the probable formation of hardpan at the Mindolo site in the future may result in a reduction of the sulfide oxidation rate. Furthermore, formation of hematite with incorporated Cu and Co will have a positive impact on the environment because hematite is very resistant to dissolution and the resulting pore water metal concentrations will be very low.

Results of the study highlight the importance of gangue rock composition already observed at mining sites around the world. When fast-acting neutralization minerals are available, there is not development of acid mine drainage and environmental impact of mining wastes is limited.

Acknowledgements

The funding for this study was provided by the Czech Science Foundation (GACR 205/08/0321/1) and Ministry of Education, Youth and Sports (MSM 0021620855). A number of colleagues helped with analytical work: Dr. Ondřej Šebek (FAAS measurement), Dr. Petr Drahota (XRD measurement, XRF measurement) M. Fayadová (laboratory assistance). We also thank Alphed Dokowe from the Geological Survey of Zambia for his assistance in the field. We thank Dr. John Molson from Université Laval for help with of editing early version of the manuscript. We also thank two anonymous reviewers, whose comments helped to improve the manuscript.

References

Binda, P.L., 1994. Stratigraphy of Zambian Copperbelt orebodies. J. Afr. Earth Sci. 19, 251–264.

Blowes, D.W., Reardon, E.J., Cherry, J.A., Jambor, J.L., 1991. The formation and potential importance of cemented layers in inactive sulfide mine tailings. Geochim. Cosmochim. Acta 55, 965–978.

Blowes, D.W., Jambor, J.L., Hanton-Fong, C.J., Lortie, L., Gould, W.D., 1998. Geochemical, mineralogical and microbiological characterization of a sulphide-bearing carbonate-rich gold-mine tailings impoundment, Joutel, Québec. Appl. Geochem. 13 (6), 687–705.

Blowes, D.W., Ptacek, C.J., Jambor, J.L., Weisener, C.G., 2003. The geochemistry of acid mine drainage. In: Lollar, B.S. (Ed.), Environmental Geochemistry, Treatise on Geochemistry, vol. 9. Elsevier, pp. 149–204.

Coats, J.S., Mosley, J.M., Mankelow, J.M., Mwale, M., Chikambwe, E.M., Muibelya, K.C., Ndhlovu, F., Nzabara, F., 2001. The Geology and Mineral Resources of Zambia, Memoir No. 6. Geological Survey Department, Ministry of Mines and Minerals development, Lusaka.

Dokoupilová, P., Sracek, O., Losos, Z., 2007. Geochemical behaviour and mineralogical transformations during spontaneous combustion of a coal waste pile in Oslavany, Czech Republic. Mineral. Mag. 71 (4), 443–460.

Dold, B., Fontboté, L., 2001. Element cycling and secondary mineralogy in porphyry copper tailings as a function of climate, primary mineralogy, and mineral processing. J. Geochem. Explor. 74, 3–55.

Gieré, R., Sidenko, N.V., Lazareva, E.V., 2003. The role of secondary minerals in controlling the migration of arsenic and metals from high-sulfide wastes (Berikul gold mine, Siberia). Appl. Geochem. 18, 1347–1359.

Gilbert, S.E., Cooke, D.R., Hollings, P., 2003. The effects of hardpan layers on the water chemistry from the leaching of pyrrhotite-rich tailings material. Environ. Geol. 44, 687–697.

Hossner, L.R., Doolittle, J.J., 2003. Iron sulfidic oxidation as influenced by calcium carbonate application. J. Environ. Qual. 32, 773–780.

Jambor, J.L., 1994. Mineralogy of sulfide-rich tailings and their oxidation products. In: Jambor, J.L., Blowes, D.W. (Eds.), Short Course Handbook on Environmental Geochemistry of Sulfide Mine Wastes, vol. 22. Mineralogical Association of Canada, pp. 59–102.

Jambor, J.L., 2003. Mine-waste mineralogy and mineralogical perspectives on acid–base accounting. In: Jambor, J.L., Blowes, D.W., Ritchie, A.I.M. (Eds.), Environmental Aspects of Mine Wastes. Short Course Series, vol. 31. Mineralogical Association of Canada, pp. 117–145.

Johnson, R.H., Blowes, D.W., Robertson, W.D., Jambor, J.L., 2000. The hydrogeochemistry of the Nickel Rim mine tailings impoundment, Sudbury, Ontario. J. Contam. Hydrol. 41 (1–2), 49–80.

Langmuir, D., 1997. Aqueous Environmental Geochemistry. Prentice Hall, Upper Saddle River, New Jersey. 600 pp.

Lefebvre, R., Hockley, D., Smolensky, J., Gelinas, P., 2001. Multiphase transfer processes in waste rock piles producing acid mine drainage 1: conceptual model and system characterization. J. Contam. Hydrol. 52, 137–164.

Lin, Z., 1997. Mobilization and retention of heavy metals in mill-tailings from Garpenberg sulfide mines, Sweden. Sci. Tot. Environ. 198, 13–31.

Lottermoser, B.G., Ashley, P.M., 2006. Mobility and retention of trace elements in hardpan-cemented cassiterite tailings, north Queensland, Australia. Environ. Geol. 50, 835–846.

McGowan, R.R., Roberts, S., Boyce, A.J., 2006. Origin of the Nchanga copper–cobalt deposits of the Zambian Copperbelt. Miner. Deposita 40, 617–638.

McGregor, R.G., Blowes, D.W., Jambor, J.L., Robertson, W.D., 1998. The solid-phase controls on the mobility of heavy metals at the Copper Cliff tailings area, Sudbury, Ontario, Canada. J. Contam. Hydrol. 33 (3–4), 247–271.

McGregor, R.G., Blowes, D.W., 2002. The physical, chemical and mineralogical properties of three cemented layers within sulfide-bearing mine tailings. J. Geochem. Explor. 76, 195–207.

Mendelsohn, F., 1961. The Geology of the Northern Rhodesian Copperbelt. Macdonald and Co., London. 523 p.
Moncur, M.C., Ptacek, C.J., Blowes, D.W., Jambor, J.L., 2005. Release, transport and attenuation of metals from an old tailings impoundment. Appl. Geochem. 20, 639–659.
Nicholson, R.V., Gillham, R.W., Reardon, E.J., 1990. Pyrite oxidation in carbonate-buffered solution: 2. Rate control by oxide coatings. Geochim. Cosmochim. Acta 54, 395–402.
Parkhurst, D.L., Appelo, C.A.J., 1999. User's Guide to PHREEQC: A Computer Program for Speciation, Reaction-path, 1-D Transport, and Inverse Geochemical Calculations. US Geological Survey Water-Resources Investigations Report 99-4259.
Petterson, U.T., Ingri, J., 2001. The geochemistry of Co and Cu in the Kafue River as it drains the Copperbelt mining area, Zambia. Chem. Geol. 177, 399–414.
Porada, H., Berhorst, V., 2000. Toward a new understanding of the Neoproterozois-Early Palaeozoic Lufilian and northern Zambezi Belts in Zambia and the Denocratic Republic of Congo. J. Afr. Earth Sci. 30, 727–771.
Rainaud, C., Masters, S., Armstrong, R.A., Phillips, D., Robb, L.-J., 2002. Contributions to the geology and mineralization of the Central African Copperbelt: IV. Monazite U–Pb dating and 40Ar–39Ar thermochronology of metamorphic events during the Lufilian orogeny. In: Miller, R.E. (Ed.), 11th Quadrennial IAGOD Symposium and Geocongress 2002. Extended Abstracts. Geological Survey of Namibia, Windhoek, Namibia, pp. 231–233.
Rainaud, C., Masters, S., Armstrong, R.A., Robb, L.J., 2005. Geochronology and nature of the Palaeoproterozoic basement in the Central African Copperbelt (Zambia and the Democratic republic of Kongo), with regional implications. J. Afr. Earth Sci 42, 1–32.
Rauret, G., Lopez-Sanchez, J.F., Sahuquillo, A., Rubio, R., Davidson, C., Ure, A., Quevauviller, P., 1999. Improvement of the BCR three step sequential extraction procedure prior to the certification of new sediment and soil reference materials. J. Environ. Monit. 1, 57–61.
Ritchie, A.I.M., 1994. Rates of mechanisms that govern pollutant generation from pyritic wastes. In: Alpers, C.N., Blowes, D.W. (Eds.), ACS Symposium Series. American Chemical Society, Washington, DC.
Romero, F.M., Armienta, m.A., Villasenor, G., Gonzáles, J.L., 2006. Mineralogical constraints on the mobility of arsenic in tailings from Zimapán, Hidalgo, Mexico. Int. J. Environ. Pollut. 26, 23–40.
Romero, F.M., Armienta, M.A., Gonzales-Hernandez, G., 2007. Solid-phase control on the mobility of potentially toxic elements in an abandoned lead/zinc tailings impoundment, Taxco, Mexico. Appl. Geochem. 22, 109–127.
Salmon, S.U., Malmström, M.E., 2004. Geochemical processes in mill tailings deposits: modelling of groundwater composition. Appl. Geochem. 19, 1–17.
Salzsauer, K.A., Sidenko, N.V., Sheriff, B.L., 2005. Arsenic mobility in alteration products of sulphides-rich, arsenopyrite-bearing mine wastes, Snow Lake, Manitoba, Canada. Appl. Geochem. 20, 2303–2314.
Smuda, J., Dold, B., Friese, K., Morgenstern, P., Glaesser, W., 2007. Mineralogical and geochemical study of element mobility at the sulfide-rich Excelsior waste rock dump from the polymetallic Zn–Pb–(Ag–Bi–Cu) deposit, Cerro de Pasco, Peru. J. Geochem. Explor. 92, 97–110.
Sracek, O., Choquette, M., Gélinas, P., Lefebvre, R., Nicholson, R.V., 2004. Geochemical characterization of acid mine drainage from a waste rock pile, Mine Doyon, Québec, Canada. J. Contam. Hydrol. 69, 45–71.
Stalker, T.W., 1994. Chambishi Mine – MS, Biennial Geological Report Covering 1st April 1992 to 1st March 1994. Nkana Division, ZCCM Limited, Kitwe.
Strömberg, B., Banwart, S., 1999. Weathering kinetics of waste rock from the Aitik copper mine, Sweden: scale dependent rate factors and pH controls in large column experiments. J. Contam. Hydrol. 39 (1–2), 59–89.
von der Heyden, C.J., New, M.G., 2004. Sediment chemistry: a history of mine contaminant remediation and an assessment of processes and pollution potential. J. Geochem. Explor. 82, 35–57.
von der Heyden, C.J., New, M.G., 2005. Differentiating dilution and retention processes in mine effluent remediation within a natural wetland on the Zambian Copperbelt. Appl. Geochem. 20, 141–1257.
Xu, N., Hochella Jr., M.F., Brown Jr., G.E., Parks, G.A., 1996. Co(II) sorption at the calcite–water interface: I. X-ray photoelectron spectroscopic study. Geochem. Cosmochim. Acta 58, 553–566.